
Environmental Conditions Impacting Late-Summer Sea Ice Concentration Predictability in the Northwest Passage

Kyle Obremski

A Thesis submitted in partial fulfillment of
the requirements for the degree of

Master of Science

(Atmospheric and Oceanic Sciences)

at the

UNIVERSITY OF WISCONSIN-MADISON


August 2024

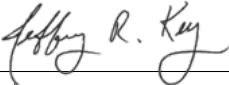
Thesis Declaration and Approval

I, Kyle Obremski, declare that this Thesis titled 'Environmental Conditions Impacting Late-Summer Sea Ice Concentration Predictability in the Northwest Passage' and the work presented in it are my own.

Kyle Obremski		08/20/2024
Author	Signature	Date

I hereby approve and recommend for acceptance this work in partial fulfillment of the requirements for the degree of Master of Science:

Tristan L'Ecuyer		08/15/2024
Committee Chair	Signature	Date

Jeffrey Key		08/20/2024
Outside Member	Signature	Date

Yinghui Liu		8/2/2024
Outside Member	Signature	Date

Grant Petty		08/20/2024
Faculty Member	Signature	Date

Abstract

Environmental Conditions Impacting Late-Summer Sea Ice Concentration Predictability in the Northwest Passage

by Kyle Obremski

The Northwest Passage, located in the Canadian Archipelago, is a conglomerate of sea routes that connect the eastern and western sides of the North American continent. Historically, sea ice in the region has made it difficult for ships not strengthened for ice breaking to utilize the Northwest Passage. With rising temperatures, sea ice in the Arctic has decreased and is likely to continue doing so. During some years in the late-summer, the Northwest Passage has so little sea ice that it is essentially open to all forms of maritime traffic. In 2013 and 2016, the Northwest Passage had anomalously high and low August sea ice concentration (SIC), respectively. Other years with high and low average SICs are identified and various thermodynamic and dynamic environmental conditions (Two-meter temperature, zonal and meridional winds, sea ice thickness, and SIC anomalies prior to August) are composited (averaged over the high and low SIC years for each month) to determine which are likely to have impacts on SIC. Composites show differences between these two samples of high and low August SIC, especially for sea ice thickness, prior SIC, and temperature early on in the year. Correlating anomalies of these variables accumulated over a number of months directly to the August SIC anomalies for the years 1982 through 2020 shows where there are areas of strong, significant correlations. Based on composite and correlation analyses it can be deduced that strongly anomalous years of high and low SIC in the NWP in August do not differentiate themselves until the spring. A convolutional neural network is created to assist in predicting when and where sea ice concentration anomalies will occur within the Northwest Passage. The model's accuracy is largely dependent on the predictors used, and the temporal range that these predictors cover. When variables related to the radiative/heat flux at the surface are included in the training data, models based on early-year data are able to increase their average August SIC prediction accuracy in the Northwest Passage by about 5%.

Acknowledgements

I would like to thank my advisors and research mentors Jeff Key and Yinghui Liu. Their willingness to work with me and their dedication to attend weekly meetings over the course of two years not only helped me put together this thesis, but it aided me in gaining the necessary experience that is required to become a professional researcher in our field. They encouraged me to present my findings on posters and in the form of oral presentations at conferences while always being open to checking over my work and offering constructive criticism that helped me create presentations that I am proud of to this day. Additionally, I would like to thank another member of my committee, Tristan L'Ecuyer. Tristan was the one who put me into my first research position as an undergraduate (as well as my academic advisor throughout my master's journey). He has always encouraged me and offered great advice on the various projects I have been on, and I look forward to working with him more in the future. I would also like to thank Juliet Pilewskie, who was my graduate mentor on that first project that Tristan put me on, and taught me how to navigate the world of research while also offering me advice and direction on how to navigate the maze of graduate school applications. Also a member of my graduate committee, I would like to thank Grant Petty. Dr. Petty was the first professor I ever had in the Department of Atmospheric and Oceanic Sciences (AOS), and I ended up taking several more classes with him throughout my undergraduate and graduate years. Dr. Petty also holds the record for being the author of the only book I have read twice cover to cover (*A First Course in Atmospheric Thermodynamics*). Last but not least, I would like to thank my friends within AOS. There have been many long hours studying and finishing assignments that honestly did not seem so long because of the great company I had. This work was funded by the NOAA Joint Polar Satellite System (JPSS) Program through a grant to the Cooperative Institute for Meteorological Satellite Studies (CIMSS), University of Wisconsin-Madison.

Contents

Abstract	ii
Acknowledgements	iii
Contents	iv
List of Figures	vi
List of Tables	vii
1 Introduction	1
1.1 The Northwest Passage	1
1.2 Analyzing Environmental Conditions and Prediction	5
1.3 Analyzing Environmental Conditions and Prediction	5
1.4 Goals and Guiding Questions	7
2 Data and Methods	10
2.1 Geospatial Data	10
2.1.1 NOAA/NSIDC Climate Data Record (CDR) of Passive Microwave 12.5 km Sea Ice Concentration, Version 5	10
2.1.2 Daily-Averaged Fifth generation ECMWF atmospheric reanalysis of the global climate (ERA5)	12
2.1.3 Extended Advanced Very High Resolution Radiometer Polar Pathfinder	12
2.2 Methods of Analysis	13
2.2.1 Composite Analysis	14
2.2.2 Correlation Analysis	15
2.2.3 Sea Ice Concentration Prediction	15
3 Results	17
3.1 An Open versus Closed Northwest Passage	17
3.2 Part 1: Composite Analysis	20
3.2.1 Years with High and Low Sea Ice Concentration	20
3.2.2 Temperature, Winds, MSLP, SIC, and Ice Thickness	21

	v
3.3 Part 2: Correlation Analysis	33
3.4 Composite and Correlation Analysis Summary	37
3.5 Part 3: Sea Ice Concentration Prediction	40
4 Summary and Conclusions	48
Bibliography)	53

List of Figures

1.1	Timeseries of SIC in the NWP	3
1.2	The Northwest Passage and its Routes	4
1.3	The Northwest Passage from Space	9
3.1	Freezing Degree Days 2013 vs. 2016	18
3.2	Wind Anomalies 2013 vs. 2016	19
3.3	SIC Timeseries by year (1982-2020)	21
3.4	Composite of Two-meter Temperature	24
3.5	Composite of 10-Meter Zonal Winds	25
3.6	Composite of 10-Meter Meridional Winds	27
3.7	Composite of Mean Sea-Level Pressure	28
3.8	Composite of Sea Ice Concentration	31
3.9	Composite of Sea Ice Thickness	32
3.10	Correlation: Two-meter Temperature	35
3.11	Correlation: 10-Meter Zonal Winds	35
3.12	Correlation: 10-Meter Meridional Winds	38
3.13	Correlation: Sea Ice Concentration	38
3.14	Correlation: Sea Ice Thickness	39
3.15	Prediction: JFM Predicting August SIC	42
3.16	Prediction: MJJ Predicting August SIC	43
3.17	Prediction: JFM w/ Flux Predicting August SIC	45
3.18	Prediction: MJJ w/ Flux Predicting August SIC	47

List of Tables

2.1 Dataset Summary	13
3.1 Composite Samples	20

Chapter 1

Introduction

1.1 The Northwest Passage

The Northwest Passage (NWP) is a conglomerate of sea routes connecting Baffin Bay to the Beaufort Sea in the Canadian Archipelago (see Figure 1.2). Historically, sea ice blocks the NWP year-round to transit by vessels without hull strengthening. These low ice class vessels must request assistance from one of the few icebreakers in the region or alter their route. Due to these limitations, only 352 NWP transits have been documented as of December 2022 since the first in 1853 (Headland, 2022). However, the NWP has exhibited lower late-summer sea ice concentration (SIC) in some recent years, allowing transits by low ice class vessels (Headland 2022, Snider 2016). The year 2007 marked the first year in which satellite observed SIC was low enough for a low ice class vessel to make the transit without being severely impeded by sea ice or assisted by an icebreaker

(Headland 2022, Snider 2016). A passenger vessel, named the *Crystal Serenity*, made a voyage through the NWP in the summer of 2016 with over 1,000 passengers, marking the largest such feat to date (Snider, 2016).

Sea ice in the Arctic region has been decreasing at a rate of about 13% per decade in the late summer from 1979 to 2017 (Wei et al., 2020). Figure 1.1 shows the average SIC in August over the NWP region from 1982 through 2020 (the period of interest for this study). Additionally, the Arctic melt season has expanded by about 5 days per decade from 1979 to 2013 (Stroeve et al., 2014). Multi-year ice (MYI) has decreased substantially in the region in 2007-2020 compared to the period of 1968-2006, making it all but certain that Arctic sea ice decline in the Arctic will continue (Howell et al., 2022). With these new norms in the Arctic, there is a need to reliably predict SIC in the region for the safety of maritime transportation that will inevitably be using the NWP (Somanathan et al. 2006, Wang et al. 2022). Unites States Navy ships operating in the region will need access to both short-term and long-term sea ice forecasts of reasonable accuracy to prevent damage to vessels. Should the NWP receive more maritime traffic, any rescue efforts conducted in the region will require sea ice concentration predictions to safely reach any vessels in distress and leave the area safely. The Bering Strait would likely see more traffic due to increased trade as well, requiring Navy vessels to operate in the region. The Northwest Passage itself provides shorter shipping times from Japan to New York than the Panama Canal can offer, which will also help reduce fossil fuel emissions released by shipping vessels (Somanathan et al., 2006).

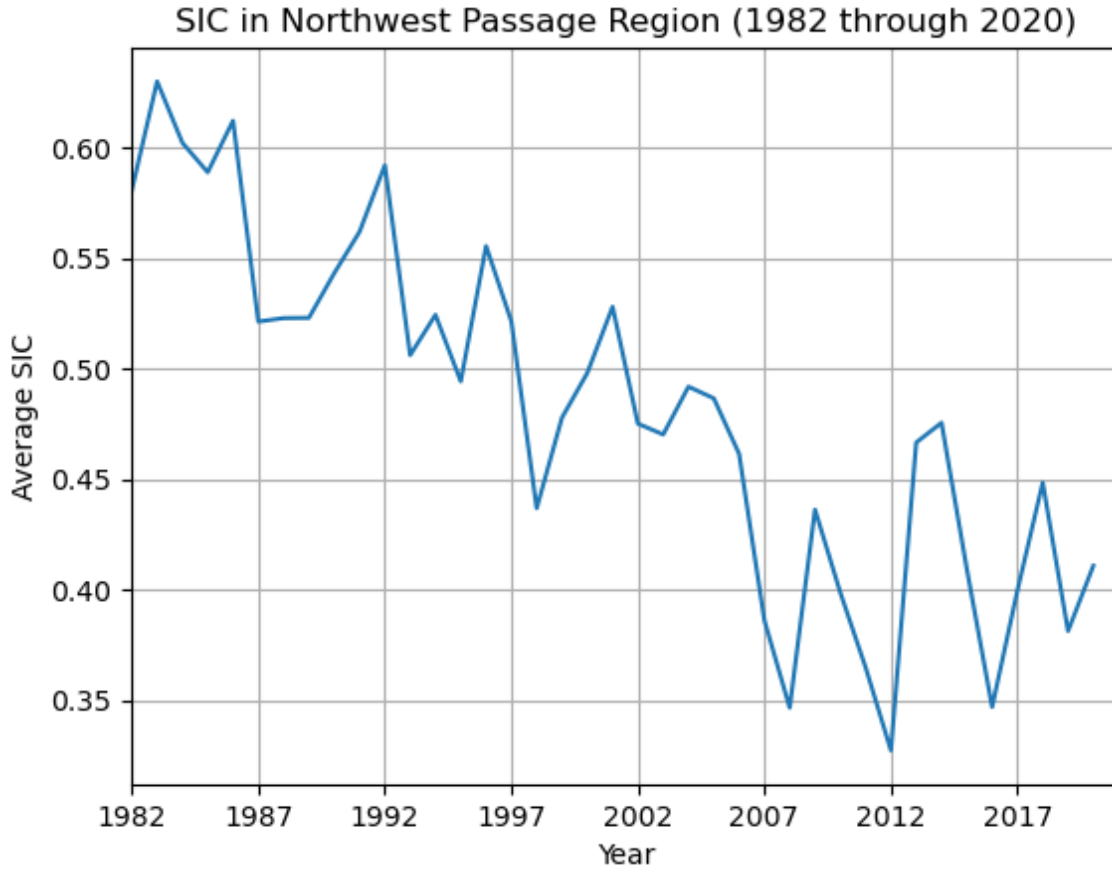


FIGURE 1.1: The average SIC from 1982 through 2020 in the Northwest Passage region in August. The study area is a bounding box roughly defined by the coordinates (latitude, longitude): (55N, 85W) in the southeast corner and (84N, 145W) in the northwest corner.

In summary, then, with more open water and a lengthened shipping season in the Arctic, understanding where sea ice will be and when it may form is a necessity. More accurate SIC predictions in the NWP will help reduce damage to ships (both Navy and private), prevent oil leaking into the Arctic environment due to damage from ice impacts, help prevent loss of life, provide valuable forecasts when planning rescue operations, and also reduce fossil fuel emissions.



FIGURE 1.2: An illustration of the Northwest Passage’s routes, major waterways, and landmasses. The Northern Route is in red, with other sub-routes in black. Base image is from Google Maps.

The NWP was observed by satellite to have first “opened” during the summer of 2007 before opening again in 2008 (Levy, 2007). The NWP being open refers to there being such a low amount of sea ice within the NWP that an open-water vessel (i.e. no ice strengthening) could conceivably navigate through the NWP without having to make large alterations to its course. The NWP in its “closed” state would signal that ice is effectively blockading the NWP to any vessels not properly strengthened for encountering sea ice. Aside from checking sea ice extent and sea ice concentrations in the region, there is yet to be an agreed upon standard for determining whether the NWP is open or closed. Figure 1.3 shows an example of the NWP being closed during August of 2013 (top of Figure 1.3) and open during August 2016 (bottom of Figure 1.3). The presence of ice in the center of the NWP in August of 2013 closes off many of the routes that are shown in Figure 1.2, but in 2016 many of the southern routes (shown in black in Figure 1.2) were open. Due to the significant cost of ice breaker use and construction and the presence of

sea ice in the NWP, it has not been feasible to utilize the NWP as a significant shipping lane (Klauz et al. 2021, Skripnuk et al. 2020). However, with Arctic warming and a decline in sea ice, it is not unreasonable to assume that maritime traffic is going to increase in the near future. In fact, Earth System Models have found it possible that even the northern routes of the NWP will be ice-free in the summer by the year 2050 (Wang et al., 2022).

1.2 Analyzing Environmental Conditions and Prediction

It is essential to understand why the NWP still sees years with higher and lower SICs as this will assist in improving predictive capabilities with respect to sea ice. By taking a closer look at the thermodynamic and dynamic environmental conditions that led up to the Augusts of 2013 and 2016, it becomes clear that conditions differ significantly when the NWP is open versus closed.

1.3 Analyzing Environmental Conditions and Prediction

In order to better understand the environmental processes that are most important to predicting SIC, composite analysis and correlation analysis are used to establish what certain environment variables' patterns are during years with low and high August sea ice. Kapsch et al. (2014) discusses the importance of spring atmospheric thermodynamic processes in initiating sea ice melt, while Yu et al. (2021) discusses how navigability of the

Northeast Passage (Russian side of the Arctic), similarly to the NWP, is greatly impacted by not just the air temperature but also the low-level winds. Though sea ice motion is often faster in the springtime when the ice is thinner, the winter sea ice motion (which is largely driven by low-level winds) has been shown to be related to summer sea ice cover as well (Kimura et al. 2013, Wang et al. 2021, Yu et al. 2021). Taking various environmental conditions into account and understanding when and where they change and begin to act on sea ice will be an important prelude to building a model with the best data utilizing machine learning methods.

SIC prediction will be done using machine learning, specifically, a convolutional neural network (CNN) will be utilized. The advantage of a CNN is its ability to take in large amounts of multidimensional geospatial data and break down the underlying patterns in order to apply what it learns to new data and make predictions (Andersson et al. 2021, Hoffman et al. 2023). In fact, Andersson et al. (2021) has shown CNNs to be an effective tool in the prediction of SIC in the Arctic. One potential obstacle in the prediction of SICs is the *Spring Barrier*, as it is referred to in Bonan et al. (2019). This term refers to the difficulty in predicting SICs in the Arctic past the spring season from earlier points in the year (before June versus after June is the cutoff). Some previous works (Zeng et al., 2023) have aimed to reduce this spring barrier in predictive models and found that including surface heat flux, cloud, or water vapor variables have the ability to improve the predictive skill of models through the spring barrier.

In this analysis, a CNN is created to predict SICs within the Northwest Passage

in August using thermodynamic and dynamic environmental data. August is chosen as the main focus for predictions because this is often when the NWP sees its lowest SICs of the year, making it likely that usage of the NWP by maritime vessels will be at its peak during the month of August. Composites of Two-meter temperature, 10-meter winds, SIC, and sea ice thickness in years with anomalous SIC in August (both positive and negative anomalies) are created to show the different environments that are conducive to SIC anomalies and how they differ in the lead-up to August. These same variables at different points in the year are then correlated directly to mean August SICs to show the strength, significance, and spatial distribution of the connections between these environmental variables and SIC. The results of this correlation analysis provide insights into the usefulness of these environmental variables as predictors in a model. CNN predictions are shown, and the accuracy of the model's predictions in the NWP are evaluated for August.

1.4 Goals and Guiding Questions

The goal of this study is to find which thermodynamic and dynamic environmental conditions have patterns that are unique to years with high average August SIC and years with low average August SIC (composite analysis), how strongly and how early anomalies of these environmental conditions are correlated to August SIC (correlation analysis), and finally, to use the information gathered about these environmental conditions/predictors to create a CNN that will predict August SICs from different points in the year. The thermodynamic and dynamic differences between 2013 and 2016 help to explain why the

NWP was open in 2016 and closed in 2013. These differences are explored in the beginning of Chapter 3 in order to set a basis for which variables to use in the composite, correlation, and CNN prediction analyses.

Using these different methods of analysis, this study will find characteristic environments with respect to Two-meter temperature, 10-meter zonal and meridional winds, sea ice thickness, and SIC prior to August. Correlations between these variables and August SIC will show how early and how strongly these variables may act as predictors for SIC. Finally, CNN predictions of SIC are tested for accuracy using these variables, and with additional variables related to the radiative/heat flux at the surface in order to overcome the spring barrier. The fundamental questions that this thesis addresses are:

1. Are there characteristic thermodynamic and dynamic environments that differentiate high August sea ice concentration years and low August sea ice concentration years? When do these environments begin to appear?
2. How strongly and how early do certain environmental variables act as predictors of August sea ice concentration in the Northwest Passage region?
3. Will a simple convolutional neural network have the ability to learn the spatial patterns that characterize where/when sea ice concentration anomalies will occur based on early season anomalies, and how will the “spring barrier” impact these predictions? Does the addition of variables relating to the radiative/heat flux help to improve these predictions?

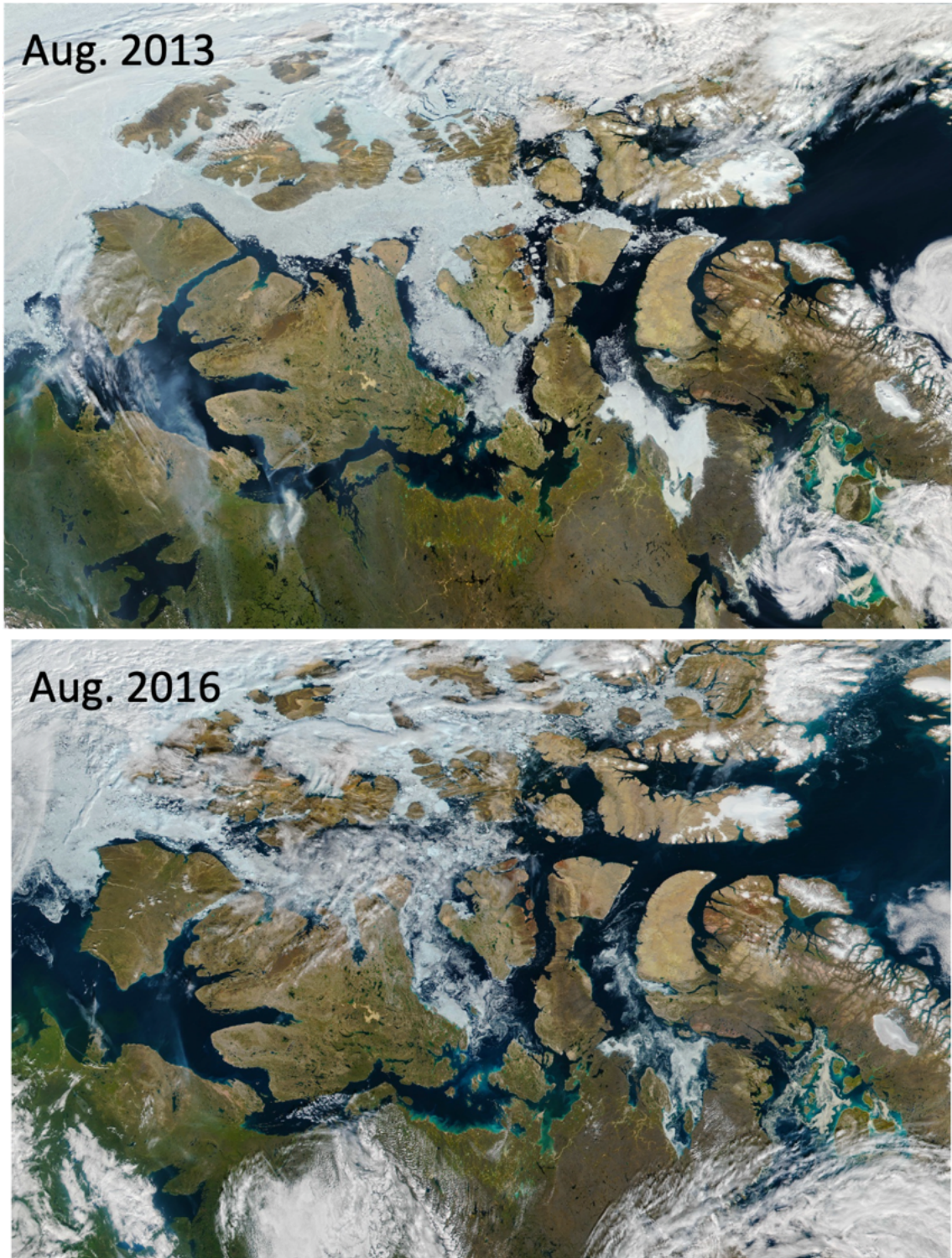


FIGURE 1.3: Image of the Northwest Passage from 2013 (top, MODIS), and 2016 (bottom, VIIRS) via the NASA Earth Observatory.

Chapter 2

Data and Methods

2.1 Geospatial Data

All geospatial data is linearly interpolated to fit the 12.5 kilometer resolution of the NOAA-CDR passive microwave SIC (version 5) product used in this analysis (see section 2.1.1). All data is detrended linearly at each grid point. The main features of the geospatial products (variables used, spatial resolution, and temporal resolution) are given in Table 2.1.

2.1.1 NOAA/NSIDC Climate Data Record (CDR) of Passive Microwave 12.5 km Sea Ice Concentration, Version 5

The region that the NWP covers is vast, making satellite remote sensing a necessary tool in observing real-time and past changes to the SIC in the region. To identify these

changes, daily SIC is measured from 1978 through 2020 (though only 1982 through 2020 is used for this analysis) using the Passive Microwave 12.5 km Sea Ice Concentration version 5 data product from the National Snow and Ice Data Center (Meier et al., 2024). With a spatial resolution of 12.5 km and daily temporal resolution over the satellite era, this data will be pivotal in observing SIC anomalies in the Canadian Archipelago. It should be noted that this version of the NOAA-CDR SIC product (version 5), is currently a beta release. Inaccuracies and discontinuities may be present in the data, particularly in the older portion. These issues have arisen due to regriding the older data to fit the 12.5 km resolution of the newer data. Upon inspection, the region of interest for this analysis was still seemingly accurate, and any values that showed severe inaccuracies were filtered out from this analysis. Any SIC values that are missing (or “NaN”), below 0.0, or above 1.0 are disregarded in this analysis. The main reason for using version 5 over version 4 is the region of interest itself. Version 5 has a resolution of 12.5 km whereas version 4 still uses a 25.0 km resolution. The Northwest Passage has many thin waterways that are likely to be better represented using the 12.5 km resolution of the version 5 product.

Another possible source of error arises when using passive microwave data during the summer months as the surface emissivity changes due to the presence of liquid water (Andersen et al., 2007). Kern et al. (2022) examines several data products and finds that SIC error may reach 20% in some cases. This error tends to lead to a negative bias in SIC retrievals during high melt conditions. However, this NOAA-CDR product utilizes two algorithms to alleviate this negative bias. The Bootstrap and NASA Team algorithms are slightly different in their usage of brightness temperature to calculate SIC, which may

lead to different values depending on the surface conditions. Due to the negative bias, SIC is calculated at each pixel by both the Bootstrap and NASA Team algorithm, but the value that makes it into the NOAA-CDR product will be the larger of the two values. There are differences, advantages, and disadvantages between various SIC products, but the main advantage of using the NOAA-CDR product is that it is one of very few daily SIC products that is updated daily throughout the entire year since November of 1978.

2.1.2 Daily-Averaged Fifth generation ECMWF atmospheric reanalysis of the global climate (ERA5)

The spatial resolution of ERA5 is 0.25° horizontal, with a daily temporal resolution covering the years from 1982 through 2020 (Hersbach and Coauthors, 2020). Two-meter temperature, 10-meter zonal winds, and 10-meter meridional winds at a daily temporal resolution were downloaded using a script created by the European Center for Medium-Range Weather Forecasts' (ECMWF) ERA5 download page. ERA5 data was linearly interpolated to fit the 12.5 km resolution of the SIC product.

2.1.3 Extended Advanced Very High Resolution Radiometer Polar Pathfinder

Daily measurements of sea ice thickness as well as all radiation fluxes used in part 3 of the analysis were gathered from the Extended Advanced Very High Resolution Radiometer (AVHRR) Polar Pathfinder (APP-x) at a 25 km horizontal resolution for the years 1982 through 2020 (Key et al., 2016). APP-x data was obtained from the NOAA Centers for

Environmental Information (NCEI). APP-x data was linearly interpolated to fit the 12.5 km resolution of the SIC product.

Dataset	Variable(s)	Spatial Resolution	Temporal Resolution
ERA-5	2-m Temperature 10-m U and V winds	0.25° (~25 km)	Daily
NOAA-CDR	Sea Ice Concentration	12.5 km	Daily
APP-x	Sea Ice Thickness Radiative Fluxes	25 km	Daily

TABLE 2.1: All dataset names, variables, spatial resolution, and temporal resolution.

2.2 Methods of Analysis

This analysis of the Northwest Passage will be split into three parts: composite analysis to understand the environmental anomalies in the lead-up to the summer for years with high sea ice anomalies and low sea ice anomalies, correlation analysis in order to establish connections between environmental conditions and late-summer sea ice concentrations, and sea ice concentration prediction to test whether a simple convolutional neural network (CNN) is able to accurately describe the locations and strength of sea ice anomalies in the Northwest Passage region based on early-season environmental information.

Throughout this analysis, accumulated (or net) anomalies will be utilized. These accumulated anomalies will be the sum of the daily anomalies over a period of time to show the overall impact an environmental variable is having on an area. For instance, an accumulated anomaly for temperature of +100 Kelvin over a period of time would signify that there is a heating surplus in that area. An accumulated anomaly for wind speed of +100 $\frac{m}{s}$ in the zonal direction would indicate that the wind has a net eastward

direction of influence. All accumulated anomalies are calculated from the first day of the earliest month for each period until the last day of the last month. For example, a February through April accumulated anomaly is calculated using daily anomalies starting February 1st all the way through April 30th and summing these daily values.

2.2.1 Composite Analysis

Using accumulated anomalies for Two-meter temperature, U and V winds, SIC, and sea ice thickness over various three month periods, the accumulated anomaly over each three month period is averaged between two samples and compared. These variables were chosen as they represent the basic thermodynamic and dynamic environmental conditions that are likely to have the greatest direct impact on SICs within the NWP. The two samples represented are years with at least 1 standard deviation ($1-\sigma$) of average SIC higher than normal and $1-\sigma$ below normal, with both being calculated over the NWP region. Compositing these variables from these two samples will show the net effect these variables will have on the environment in the lead-up to an anomalous August with respect to SIC. Characteristic environments emerge, and are then tested for significance. P-values (calculated using a standard t-test) are calculated at each pixel to show where the samples are significantly statistically different.

2.2.2 Correlation Analysis

For each year in this analysis (1982 through 2020), the accumulated anomaly of each variable of interest over various 3-month periods is calculated and correlated to the average August SIC anomaly. The Pearson correlation coefficient and P-values (using a standard t-test) are both calculated at each pixel to show the strength and significance of the correlations between each environmental variable and August SIC. The intention is to show which variables influence the August SIC and how early their influence is felt.

2.2.3 Sea Ice Concentration Prediction

Two convolutional neural networks are created to predict SIC from accumulated anomalies (the predictors) of Two-meter temperature, U and V winds, past SIC, and sea ice thickness. One model will cover the period from January through March and the other May through July. These models are created using TensorFlow (Abadi et al., 2016), and take the variables mentioned as predictors along with a target, the average SIC for each August, as inputs to their training. In all, there are 39 years (1982-2020) in the dataset, with each year having corresponding predictors and targets. The training data encompasses about 80% of the total data with the remainder used as test data, resulting in only 39 total samples with roughly 31 used for training. Although this number of samples only allows for the creation of basic neural networks, it lays the groundwork for a more advanced model to be created that incorporates more data samples in the future. Training separate models will allow each individual model to learn the important patterns and spatial anomalies from each period of interest in order to predict the resulting SIC fields.

The model architecture remains the same for both the January-March and May-July models, and the results are compared. The model architecture involves several blocks with multiple convolutional layers (for pattern recognition), pooling layers (summarizes small areas of data to help with processing and pattern recognition), and batch normalization layers (normalizes the inputs of each layer to assist the model performance). Rectified Linear Unit (ReLU) activation functions are used which remove negative values from the data, which forces the model to focus on positive values (i.e. the most important details). This model architecture also employs a combined loss function to minimize error while also making predictions look as similar to validation as possible to preserve detail (Chollet, 2021).

The two models discussed will only have five predictors as inputs, but one more model will be created with 10 predictors. This model with 10 predictors will include variables impacting the surface heat flux such as the longwave and shortwave flux oriented both up and down, and the longwave and shortwave cloud radiative effects. This model is trained on January, February, and March accumulated anomalies and will be compared to the model trained on the same time period with just five predictors. It is expected that including these additional predictors will allow the model to overcome the spring barrier that is often observed when attempting to predict SIC, and lead to an increase in SIC prediction accuracy than the model with less predictors.

Chapter 3

Results

3.1 An Open versus Closed Northwest Passage

Figure 3.1 shows the difference in Freezing Degree Days (FDD) between 2013 and 2016 for June, July, and August. FDD is calculated the same as it is in Assel (1980) by taking the freezing temperature of sea water ($\sim -1.8^{\circ}C$) and subtracting the average daily temperature and summing the resulting values over the entire period of interest (in this case 1 month periods, beginning on the first day of each month and ending after the last). High FDD values signify an environment more conducive to sea ice growth, while lower values signify an environment in which there would be more melting and/or liquid seawater.

Figure 3.1 shows that 2013 and 2016 had opposite thermodynamic environments with respect to FDD values in the Canadian Archipelago (the boxed region in Figure 3.1). 2013 saw higher FDD values and 2016 saw lower values. This indicates that the 2013 summer months were colder in the NWP than the 2016 summer months, which is likely a cause for why there is more sea ice seen in 2013 in Figure 1.3 versus the bottom image, which takes place in 2016.

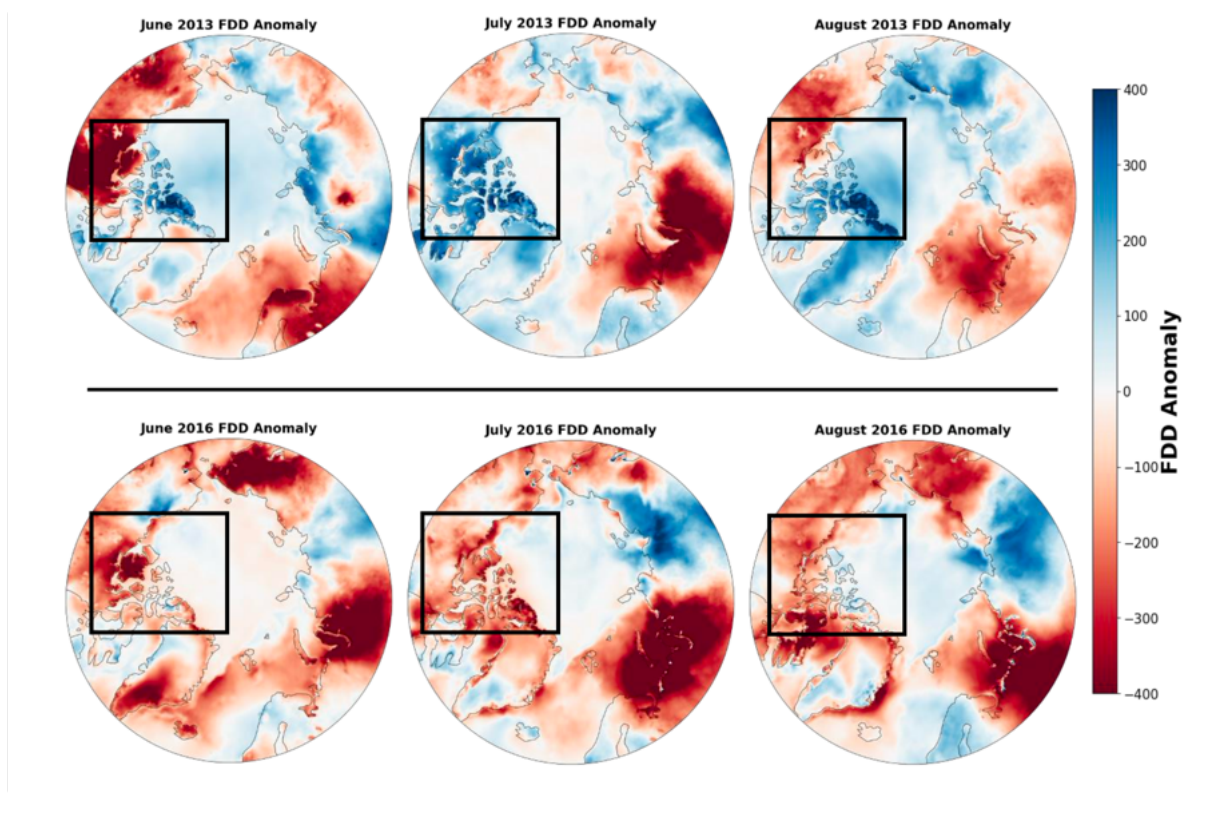


FIGURE 3.1: Graphic showing the difference between June, July, and August FDD values for 2013 (top row) and 2016 (bottom row). Boxed region is the location of the Northwest Passage (Canadian Archipelago).

Figure 3.2 shows the dynamic differences between June, July, and August of 2013 and 2016. Sea ice is transported by low-level winds, which means that the direction of the wind can be used as a proxy for the general direction of sea ice motion in most

instances (Yu et al., 2021). The 1000 hPa full wind anomaly is shown in Figure 3.2, and an interesting pattern emerges for both 2013 and 2016. 2013 sees the mean wind direction oriented towards the east (see the large blue arrow) on the western side of the Canadian Archipelago over the Beaufort Sea. This would act to transport sea ice from the Beaufort Sea region to the east, and into the NWP, raising the SICs. The opposite pattern emerges in 2016, with winds blowing north and slightly to the west, which would act to evacuate sea ice from the NWP and keep ice from entering the Canadian Archipelago.

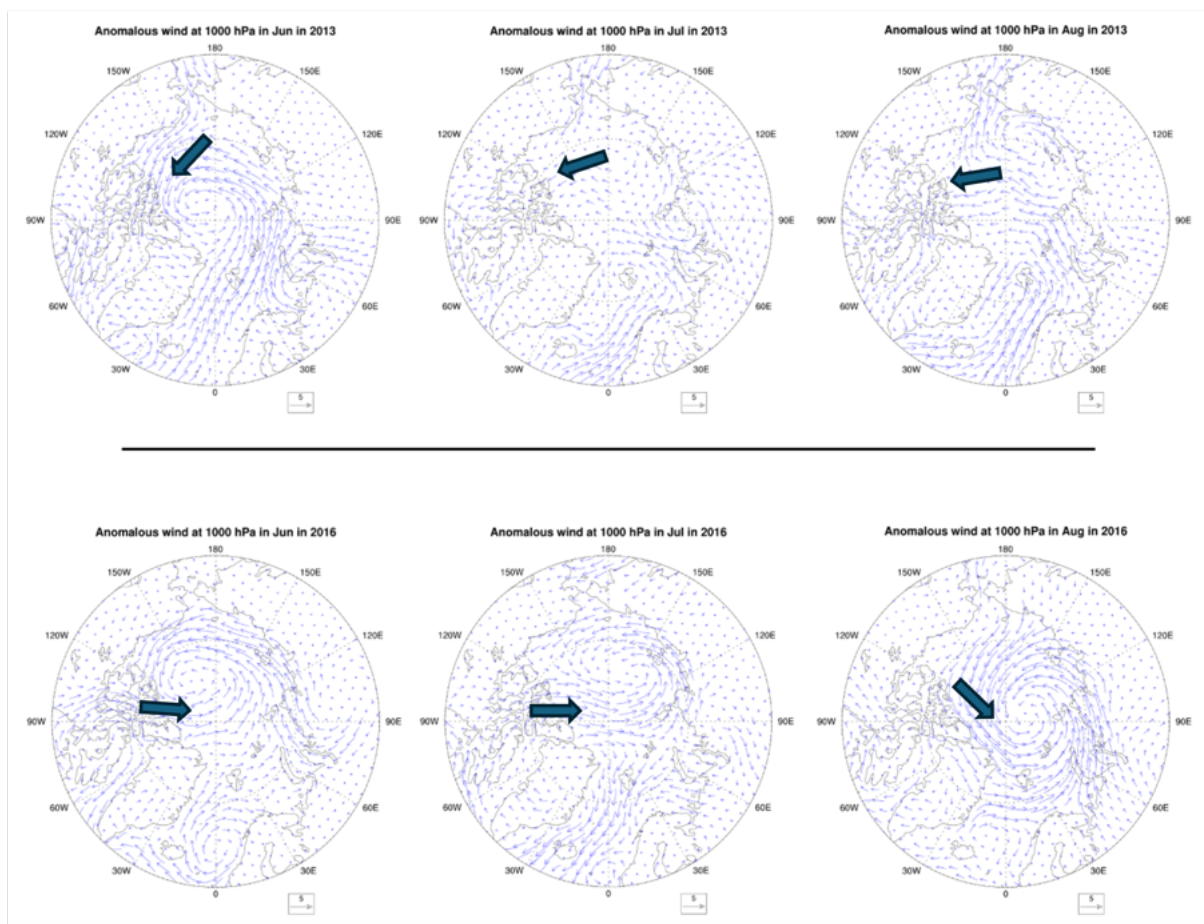


FIGURE 3.2: Graphic showing the difference between the anomalous 1000 hPa winds in June, July, and August for 2013 (top row) and 2016 (bottom row). Larger arrows indicate mean wind direction in that general location.

3.2 Part 1: Composite Analysis

3.2.1 Years with High and Low Sea Ice Concentration

In order to differentiate years in which the Northwest Passage contained more ice and less ice than normal, a cutoff of $1\text{-}\sigma$ average August SIC in the NWP region (approximately the boxed area in Figure 3.1) was used. Figure 3.3 shows the cutoffs used in dashed black lines. It also shows a timeseries from January through December of the average SIC for each month, where each individual line represents a different year from 1982 through 2020. The green lines represent the years in which the August SIC was at least $1\text{-}\sigma$ below normal, and the red lines are the years with at least $1\text{-}\sigma$ of SIC above normal across the NWP region. The grey lines are all of the other years. The green lines, the low SIC years, and the red lines, the high SIC years, represent the two samples that will be compared in this composite analysis. The specific years contained in each of these samples are listed in Table 3.1. Figure 3.3 seems to suggest that the years with very low and very high August SIC begin to differentiate themselves in the spring, given the divergence between the red lines and the green lines that seems to first appear April/May.

Low SIC Years	1998, 2007, 2008, 2011, 2012, 2016
High SIC Years	1992, 2001, 2013, 2014, 2018, 2020

TABLE 3.1: The two samples of being composited: years with high average August SIC, and those with low average August SIC in the Northwest Passage region.

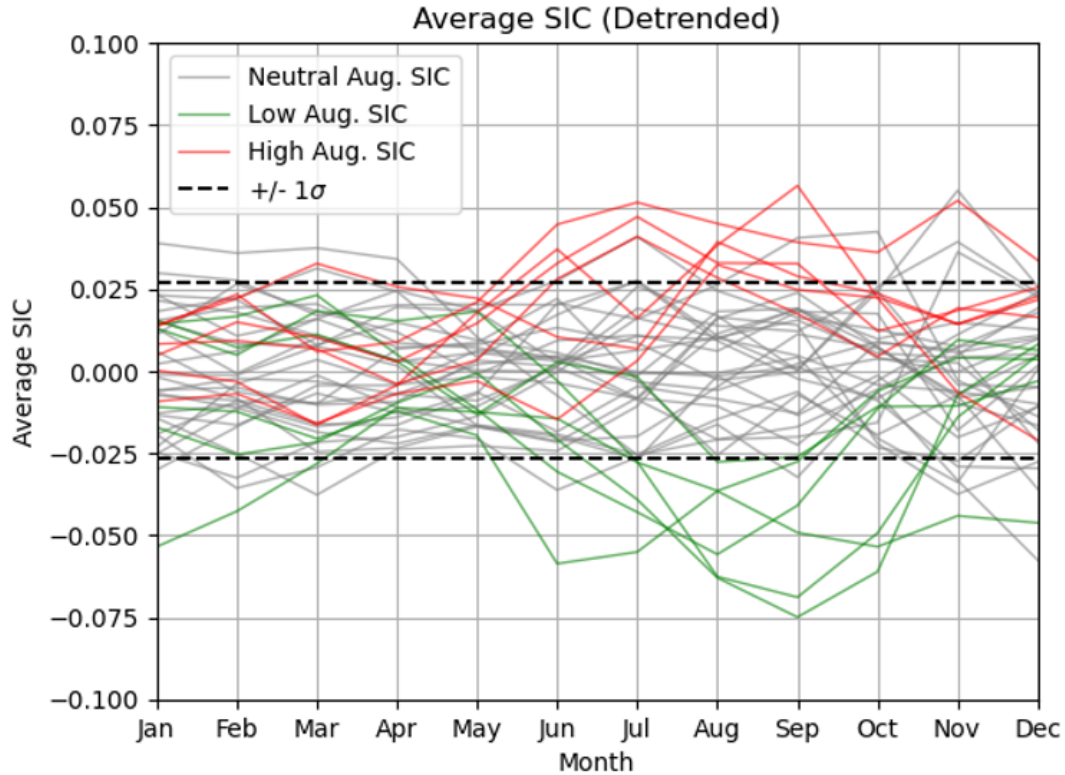


FIGURE 3.3: Detrended monthly-averaged SIC values over NWP region for each year from 1982 through 2020. The horizontal dashed lines represent the $\pm 1-\alpha$ of mean August SIC. Green lines are the timeseries for years with $-1-\alpha$ or less mean August SIC, and the red lines are the timeseries for years with $+1-\alpha$ or greater mean August SIC. Grey lines are years without significantly anomalous August SIC.

3.2.2 Temperature, Winds, MSLP, SIC, and Ice Thickness

Figure 3.4 shows the accumulated anomaly of Two-meter Temperature averaged over two samples, the Low SIC Years and High SIC Years (see Table 3.1), over six different 3 month periods. The temperature anomaly is summed up over these three months for each year before being averaged over all years present in the sample. Stippling represents areas where there is a significant difference between the two samples and where the P-values are calculated as being 0.05 or less (95% significance level). Red areas signify a

temperature surplus, and blue areas a temperature deficit.

In the earliest time period within Figure 3.4, January through March, starts to show a slight temperature difference between the years with low August SIC and high August SIC, but significant area is largely not present. In February through April, this pattern of higher temperatures in the low SIC years and lower temperatures in high SIC years starts to become clearer, but without large significant areas. March through May is where significant areas begin to appear in larger areas, specifically over the Greenland landmass and over the Beaufort Sea. April through June sees magnitudes of temperature surpluses and deficits increase and a further expansion of significant area into the southwestern waters where the Beaufort Sea and the Amundsen Gulf meet and over the Canadian continent. From this point, the two samples are almost completely opposite. May through July shows a stark difference between the low August SIC years and the high SIC years. Significant areas cover almost the entire Greenland landmass and each landmass within the Canadian Archipelago. Interestingly, the significant areas and highest magnitudes of temperature difference occur over land in May through July before showing significant differences over water within the Canadian Archipelago in June through August. Land heats faster than water and conducts heat into the water, which seems to be the reason for this lag between when land first shows significant differences in temperature versus water between the two samples. Although the SIC differences occur in August over water, the warm/cold landmasses within the Canadian Archipelago earlier in the year will likely impact water temperature and SIC in the summer as well. Overall, differences in the heat budget of high and low August SIC years in Figure 3.4 hint to an environmental

difference early in the year, but the statistically significant differences seem to take shape in late spring and strengthen in the summer months.

Figure 3.5 shows the accumulated anomaly of the 10-meter zonal wind over 3 month periods averaged over the low August SIC years (left column) and high August SIC years (right column). In this case, positive (red) values would indicate a net eastward effect of the zonal wind and negative (blue) values a net westward effect. Winds act to transport sea ice, therefore directly impacting the SIC (Kimura et al. 2013, Wang et al. 2021, Yu et al. 2021). Similarly to Figure 3.4, Figure 3.5 begins to show a pattern of difference between the two samples that strengthens as the summer months get closer. In January through March, February through April, and March through May the pattern of a net westward wind over the southwestern Canadian Archipelago, near the Amundsen Gulf and Beaufort Sea, begins to increase in magnitude and become a clear feature in the low August SIC sample with a net Eastward effect of the winds in the high August SIC side. Although this area of difference between the two samples begins to form earlier in the year, significant differences between the samples do not seem to appear until the April through June period. However, during this period the differences are stark, with the two samples becoming opposite in terms of the zonal wind direction. June through August shows a similar pattern to May through July. The effect of these opposite wind impacts is that in the low August SIC years there is a net westward impact by the zonal winds which would likely act to push sea ice out of the NWP region, lowering SICs. The high August SIC years display a net eastward impact of the zonal winds which would likely lead to sea ice entering the NWP region from the west, raising the SICs in the area.

Northwest Passage Net 2-Meter Temperature Anomaly Averages

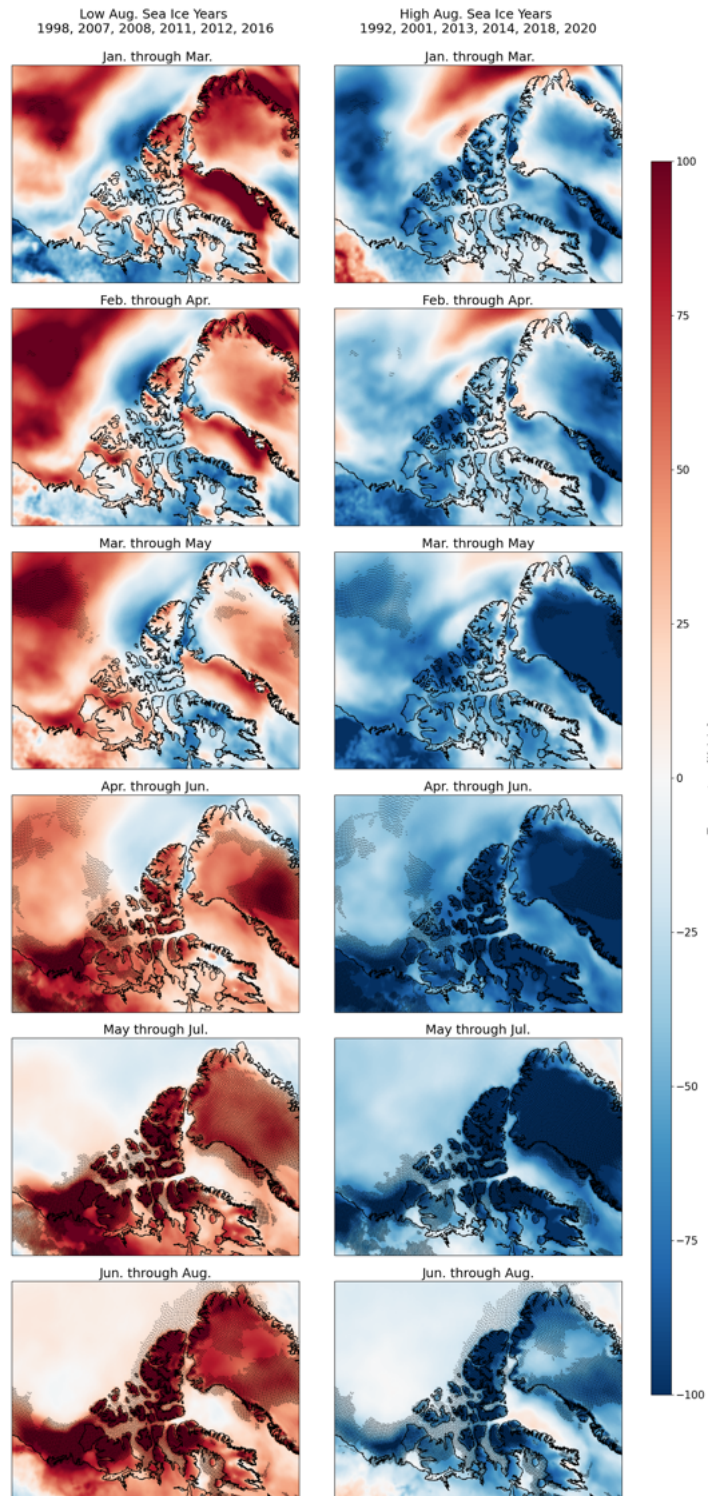


FIGURE 3.4: Composite of 2-m Temperature for low mean August SIC years (left column) and high mean August SIC years (right column) for various 3-month periods. Stippling is where p -values ≤ 0.05 .

Northwest Passage Net 10-Meter Zonal Wind Anomaly Averages

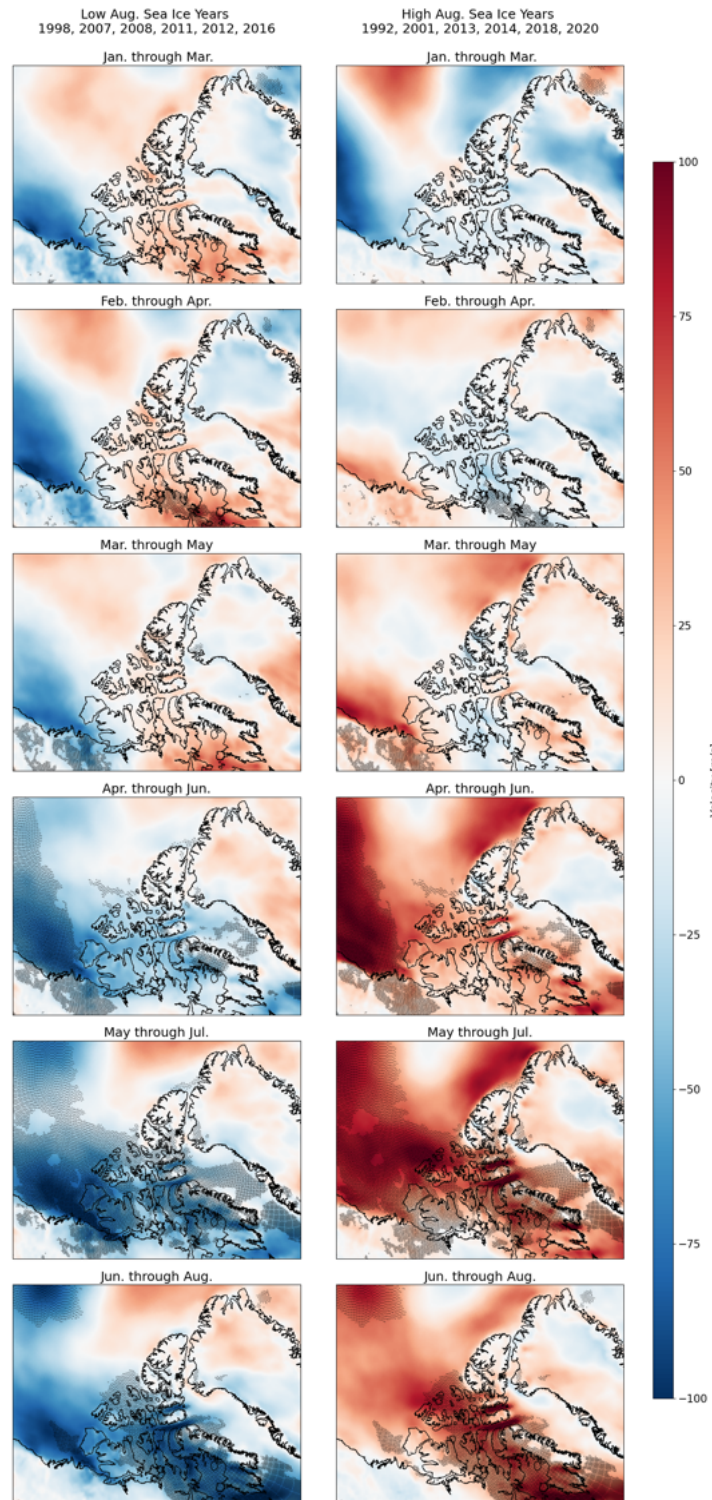


FIGURE 3.5: Composite of 10-m Zonal Winds for low mean August SIC years (left column) and high mean August SIC years (right column) for various 3-month periods. Stippling is where p -values ≤ 0.05 .

Figure 3.6 shows the accumulated anomaly of the 10-meter meridional wind over 3 month periods averaged over the low August SIC years and high August SIC years. Positive (red) values mean that the meridional wind has a net northward impact, and negative (blue) values show a net southward impact. Unlike the zonal wind in Figure 3.5, the meridional wind does not show a clear pattern of difference between the two samples. In April through June, an area of positive values begins to develop over the Beaufort Sea in the Northwest, but this area is present in both samples and continues over the next couple of periods as well. Significant areas of difference are very few and very small in area when they do show up, suggesting that there is not much variability between the two samples with respect to the meridional winds. Overall, Figure 3.6 suggests that the meridional winds are not a variable that will differentiate the low August SIC years from the high August SIC years.

Figure 3.7 shows the accumulated anomaly of Mean Sea-Level Pressure (MSLP) over various 3 month periods that are averaged over the two samples. Positive (red) values indicate a higher anomaly of MSLP and lower (blue) values indicate a lower anomaly. Although MSLP is not used further in this analysis, it is an interesting variable to look at due to its impact on the winds. A difference in MSLP between the two samples does not seem to appear until the April through June period. However, the April through June period shows a large portion of significant area and opposite MSLP values between the two samples. This larger area covers a large portion of the northern half of the NWP and extends west over a large area of the Beaufort Sea. Over the next two periods, this large area of anomalous MSLP shifts to the east until it is centered over the Greenland

Northwest Passage Net 10-Meter Meridional Wind Anomaly Averages

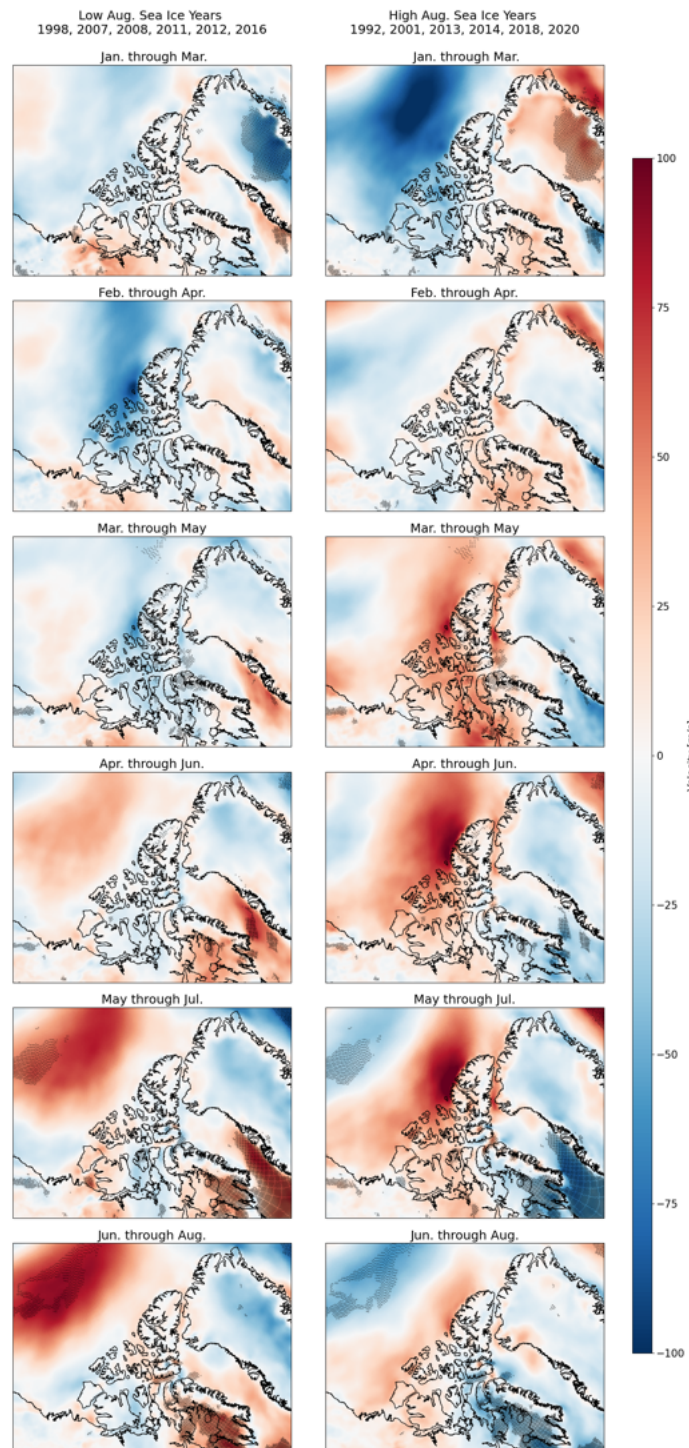


FIGURE 3.6: Composite of 10-m Meridional Winds for low mean August SIC years (left column) and high mean August SIC years (right column) for various 3-month periods. Stippling is where p -values ≤ 0.05 .

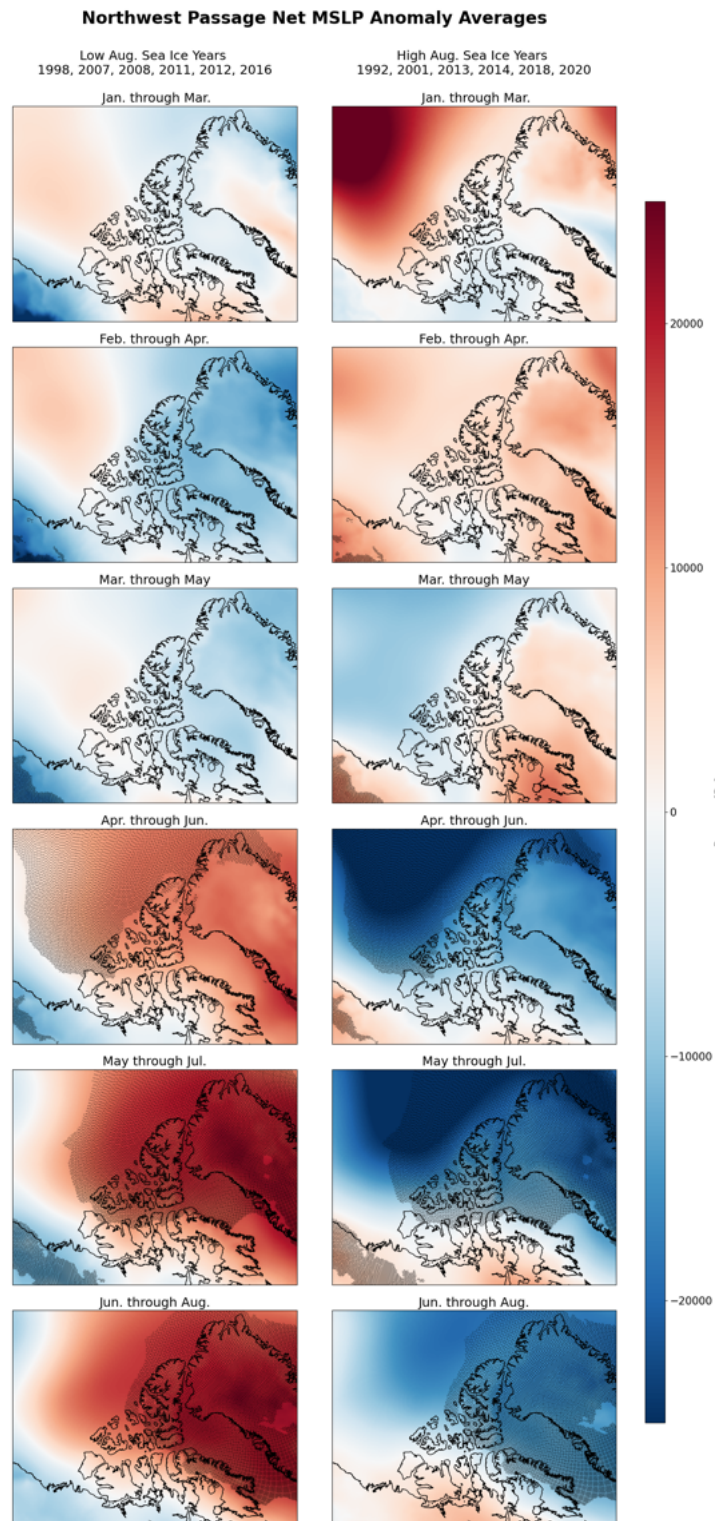


FIGURE 3.7: Composite of MSLP for low mean August SIC years (left column) and high mean August SIC years (right column) for various 3-month periods. Stippling is where p -values ≤ 0.05 .

landmass. This large pressure anomaly directly influences the orientation of the winds that are observed in Figure 3.5 and Figure 3.6. The positive anomalies in MSLP observed in the low August SIC years would lead to an anti-cyclonic (clockwise) wind pattern that would cause winds to blow to the west from the NWP, moving sea ice out of the area. The opposite is true for the high August SIC years as there is a cyclonic (counterclockwise) wind pattern that would be present. This would lead to sea ice being transported into the NWP from the west. Figure 3.7 gives insight into why the wind patterns in the zonal and meridional components of the 10-meter winds look the way that they do between these samples and suggests that anti-cyclonic pressure patterns over the NWP would lead to lower SICs whereas cyclonic pressure patterns in the region would lead to higher SICs.

Figure 3.8 shows the accumulated anomaly of SIC averaged for each of the two samples. Positive (red) values would indicate a surplus of SIC over the 3-month period and negative (blue) values would mean a SIC deficit. The first two periods, January through March and February through April, do not show a large difference in accumulated anomaly of SIC, likely because this early in the year the SICs are at, or close to, 100% and are relatively constant. Once spring is included in the March through May period, a significant difference between the two samples in the southwestern Canadian Archipelago begins to present itself. There is an SIC deficit in the low SIC sample and a surplus in the high SIC sample. This area grows in significance, magnitude, and area as time passes. April through June, May through July, and June through August show the evolution of these differences. April through June shows these anomalies encompassing more area to the north in the Beaufort Sea. In May through July, differences within most routes of

the NWP begin to show, and by June through August it is apparent that SIC varies by a substantial amount from the low August SIC years to the high August SIC years. It is interesting that significant SIC differences begin to show up slightly earlier than the significant areas of both the winds and temperature.

Figure 3.9 shows the accumulated anomaly of sea ice thickness averaged over the two samples for various 3 month periods. Positive (red) values indicate increased thickness and negative (blue) values indicate decreased thickness. Unlike all of the other variables, there seems to be an apparent pattern showing in the earliest period, January through March. Just off of the southwestern edge of the Canadian Archipelago (west of Banks Island), significant area is present, although the differences in magnitude between the decreased and increased thicknesses are only slight. The decreased thickness in the low SIC years and the increased thickness in the high SIC years is not very large in February through April either, but statistically significant area remains. March through May shows the significant area grows slightly and the magnitudes of the thickness anomalies become more apparent. April through June and May through July shows that these anomalies get even greater in magnitude, and by the June through August period that entire southwestern edge opposite between the samples with some more area showing higher magnitudes of anomalies to the east, specifically within the Northern Route of the NWP. Even compared to the accumulated anomaly of SIC in Figure 3.8, the accumulated anomaly of sea ice thickness seems to present itself early. Sea ice thickness is the variable that shows the greatest difference between low August SIC years and high August SIC years at the earliest point in the year.

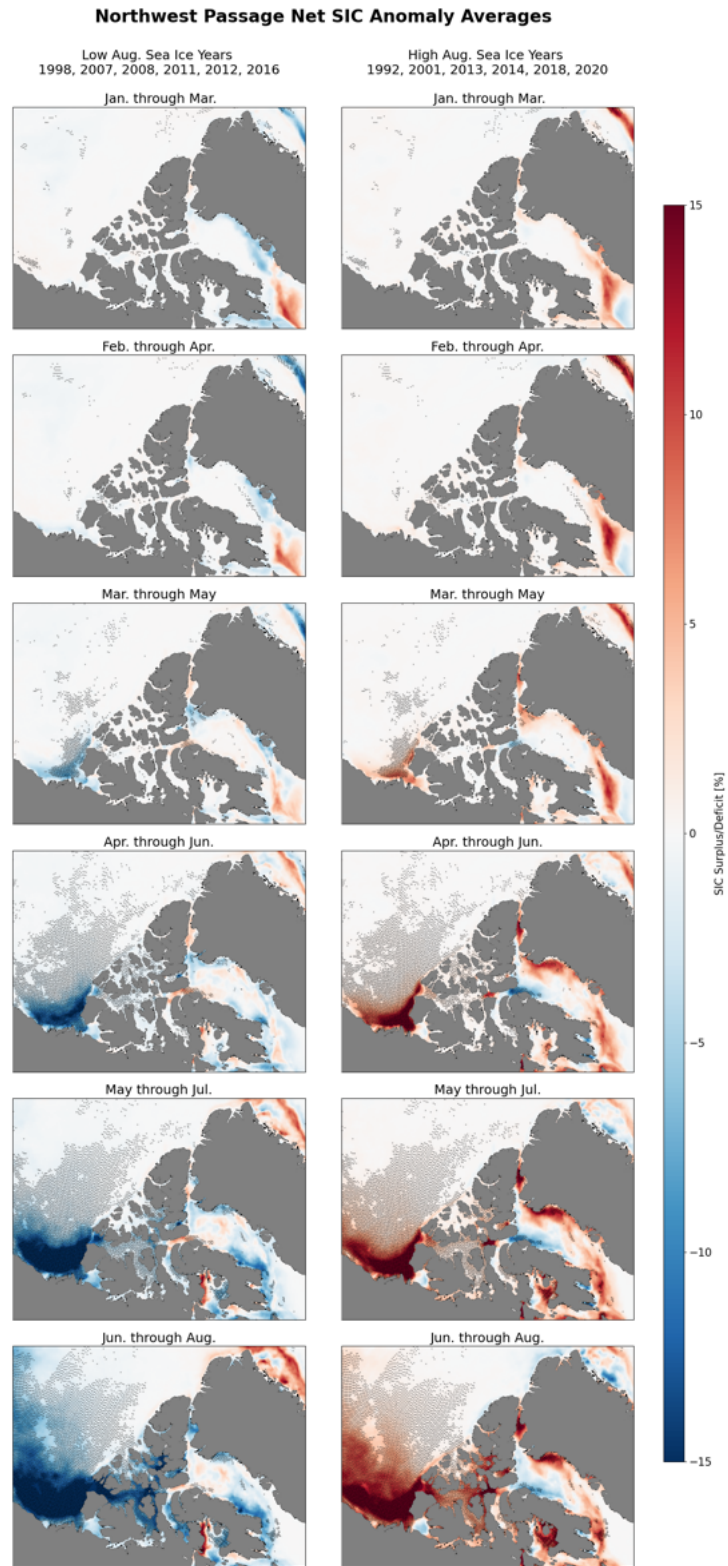


FIGURE 3.8: Composite of SIC for low mean August SIC years (left column) and high mean August SIC years (right column) for various 3-month periods. Stippling is where $p\text{-values} \leq 0.05$.

Northwest Passage Net Sea Ice Thickness Anomaly Averages

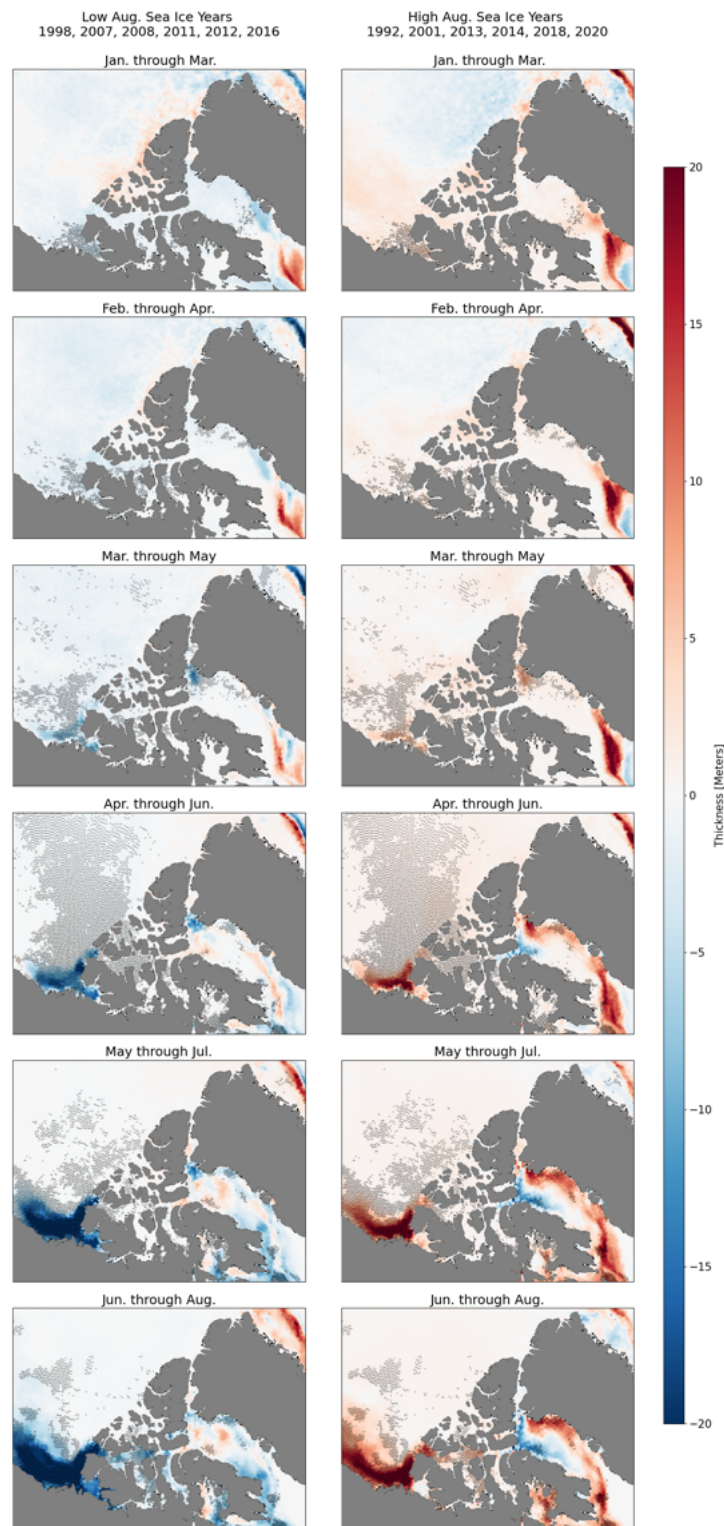


FIGURE 3.9: Composite of Sea Ice Thickness for low mean August SIC years (left column) and high mean August SIC years (right column) for various 3-month periods. Stippling is where p -values ≤ 0.05 .

3.3 Part 2: Correlation Analysis

Establishing differences between years with low August SIC and high August SIC was crucial in determining whether accurate prediction of SIC is possible. The Composite Analysis showed that most of the variables of interest show opposite effects on each sample. These environmental conditions are now tested for their correlation directly to the August SIC anomalies. This will give insight into which of these variables may best be used as predictors, and which would make the most sense to include in a model aimed at predicting SICs.

Figure [3.10](#) shows a correlation of the accumulated anomaly of the Two-meter temperature to the mean August SIC anomalies for the years 1982 through 2020 over various 3-month periods from January through August. In this case, positive (red) values mean a positive correlation and the negative (blue) values signal a negative correlation. Stippling represents the locations where the P-values are 0.05 or less, or where there is 95% confidence that the correlation is significant. In the case of the Two-meter temperature, there are widespread negative correlations, which makes perfect sense because as temperatures rise, SIC would fall, and as temperatures fall, SIC would rise. The January through March period already shows widespread significant area to go along with the negative correlations, including withing the NWP's routes. As the time periods progress further into the year, these negative correlations grow in magnitude, and the significant area continues to expand. In the final period, June through August, the entirety of the

maritime regions within the Canadian Archipelago are covered in significant area, with correlations ranging from -0.50 to -0.95 in most of the area.

Figure 3.11 and Figure 3.12 show the August SIC anomalies correlated with the accumulated anomalies of the zonal and meridional components of the 10-meter wind, respectively. Starting with the meridional wind, it becomes apparent that, at least for most of the year, there are no widespread patterns to speak of. However, some significant positive correlations off of the southwestern edge of the Canadian Archipelago (west of Banks Island) begin to take shape in May through July and are still present in June through August. This would signify that SIC in this area would fall with the negative direction of the wind (southward blowing) and rise with the positive direction (northward blowing). The meridional wind does not seem to be a great predictor of sea ice on its own, but its inclusion in a machine learning model may be necessary as it provides information to the model about the overall wind pattern.

Looking at the zonal wind in Figure 3.11, it is apparent that the zonal wind has widespread positive correlations with August SIC. Early on, in January through March, February through April, and March through May, a smaller region of positive correlations begins to form to the southwest of the Canadian Archipelago similarly to the meridional wind. However, this area shows up much earlier than the meridional wind's positive correlation and it continues to grow over the next few periods. The zone of significant positive correlations grows and strengthens with time as the area moves along the western axis of the Canadian Archipelago and starts to show up within areas of the NWP as

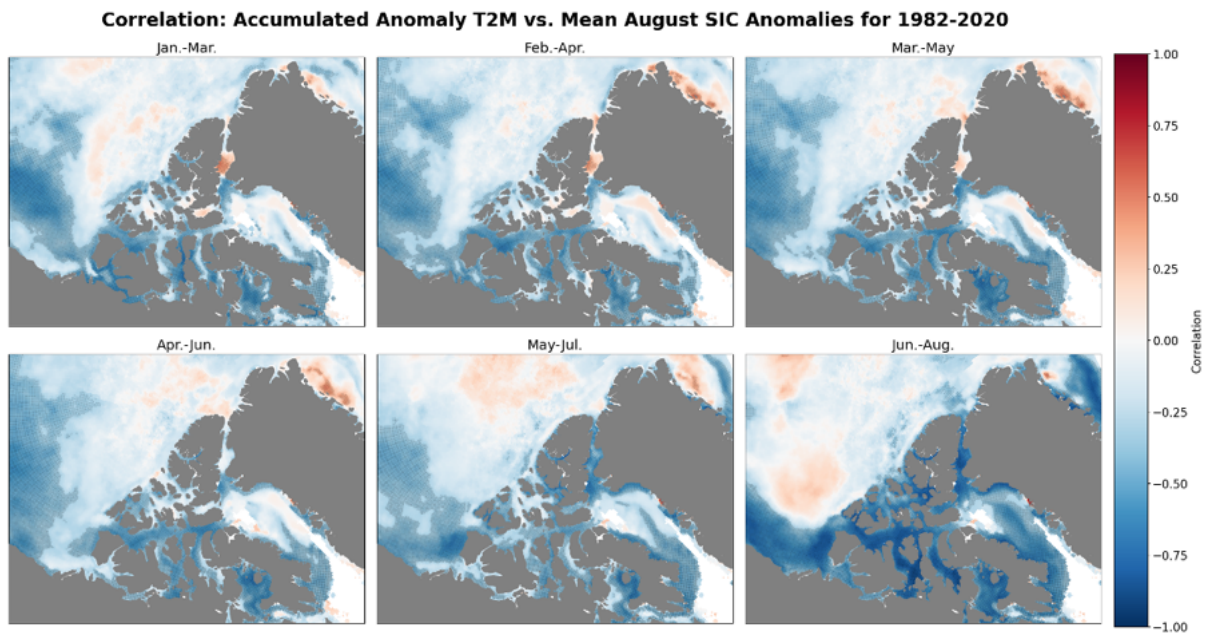


FIGURE 3.10: 2-m Temperature correlated with mean August SIC anomalies from 1982 through 2020 for various 3-month periods. Stippling is where p -values ≤ 0.05 .

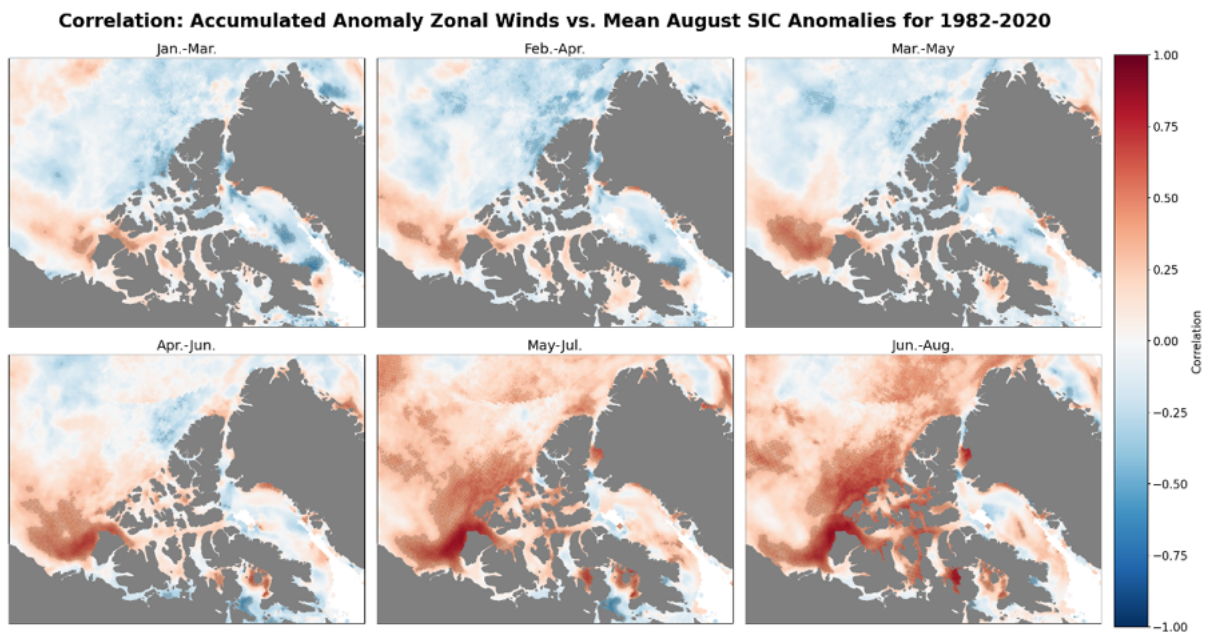


FIGURE 3.11: 10-m Zonal Winds correlated with mean August SIC anomalies from 1982 through 2020 for various 3-month periods. Stippling is where p -values ≤ 0.05 .

well. By June through August correlations reach upwards of 0.75, with the significant area reaching through most of the NWP routes. The zonal wind likely becomes more significant, and better correlated with the August SIC later in the year because the sea ice concentration is close to 100% as a consolidated ice pack in the winter months and the early spring. This would mean that the wind would need to transport large swathes of ice that would move much slower, leading to minimal change in SIC. By mid to late-spring, the sea ice is thinner, and is more easily broken apart. These smaller pieces are able to be transported easier, and SICs are raised within the NWP when the winds blow to the east, transporting sea ice into the NWP, leading to positive correlations. When the wind blows to the west (negative direction), the sea ice is transported out of the NWP, lowering SICs. This tracks well with what was observed in Figure 3.5. The zonal wind is a good predictor of SIC once the sea ice begins to break apart.

Figure 3.13 shows the correlation between the August SIC anomalies and the accumulated anomaly of SIC during various 3 month periods from 1982 through 2020. One of the most important aspects of predicting SIC is knowing the previous values of SIC in a given location. Using these accumulated anomalies of SIC, it can be deduced where SIC is already experiencing a surplus or deficit, and using this correlation strategy, it can be determined when/if a surplus/deficit of SIC becomes a good predictor of the SIC in August. Looking at Figure 3.13, specifically in the earlier periods, January through March, February through April, and March through May, it may be surprising to see that the correlations are weak and the significant area is sparse. However, just like with the winds, it is important to note that the SICs this early in the year are close to 100% and are not

shifting all that much. March through May sees significant area start to fill in off the southwestern edge of the Canadian Archipelago, but once the late-spring is included in April through June, positive correlations begin to grow in magnitude and the significant area begins to cover the area. By May through July, some of these positive correlations are reaching 0.9 and the significant area essentially covers the entire region. June through August is obviously showing the highest correlations with the most significant area as the accumulated anomaly of SIC is almost concurrent with the August SIC anomalies. The accumulated anomaly of SIC is a great predictor of SIC once the warmest months are included, but it is likely useful even in the March through May period.

3.4 Composite and Correlation Analysis Summary

Figure [3.14](#) shows the accumulated anomaly of sea ice thickness correlated with the August SIC anomalies. It is largely apparent right away that the thickness is a great predictor of August SIC even as early as January through March. The thickness grows in significant area and the correlations strengthen with time. The concentration of the area with the highest positive correlations seems to be over the Beaufort Sea, suggesting that thick ice in this region will lead to higher SICs in those areas in the summer. This may be obvious, but it is important to confirm the ability of thickness to act as a predictor of August SIC. The thickness of the sea ice is likely the best predictor out of the variables analyzed, and will be a necessary component of any machine learning model used for predicting SIC.

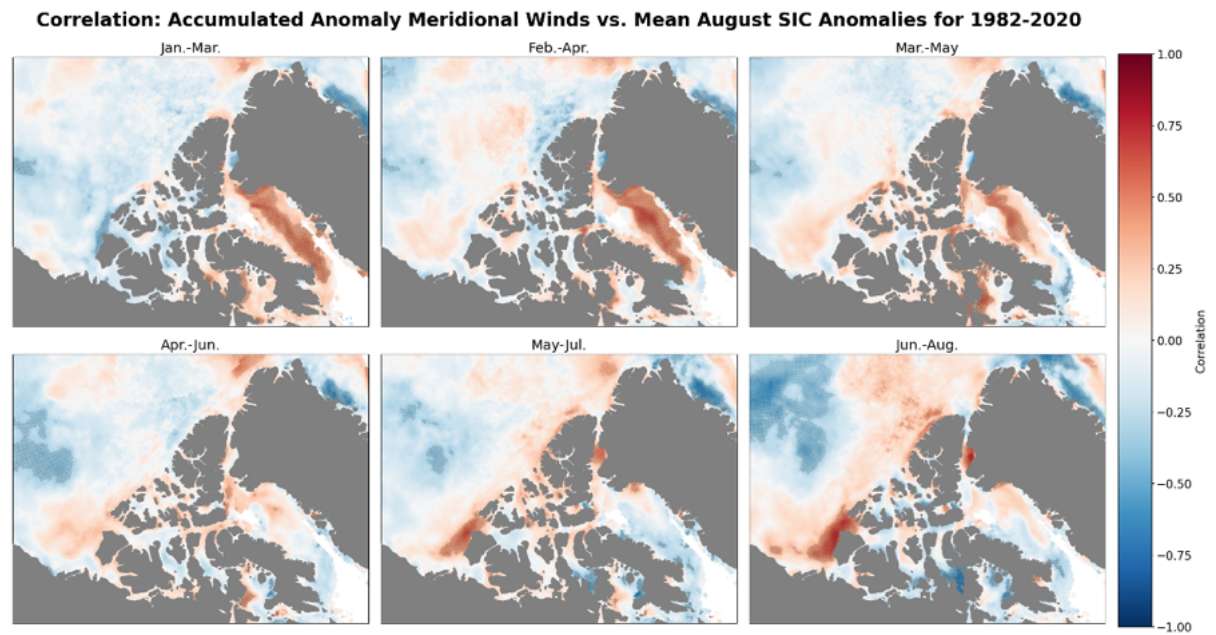


FIGURE 3.12: 10-m Meridional Winds correlated with mean August SIC anomalies from 1982 through 2020 for various 3-month periods. Stippling is where p -values ≤ 0.05 .

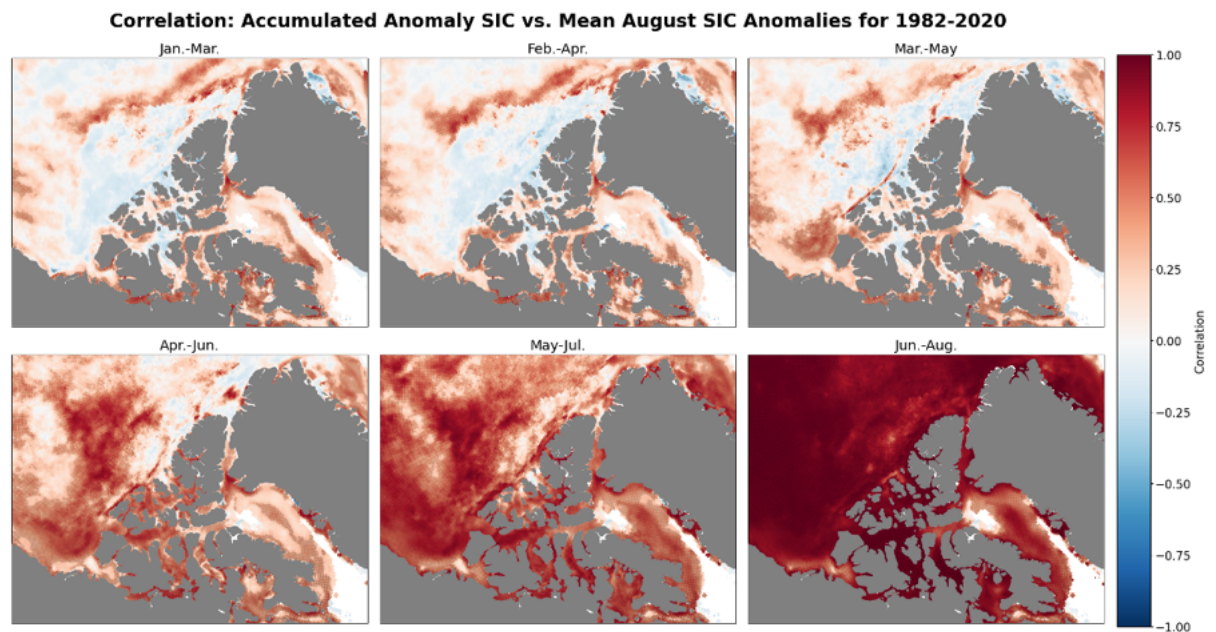


FIGURE 3.13: SIC correlated with mean August SIC anomalies from 1982 through 2020 for various 3-month periods. Stippling is where p -values ≤ 0.05 .

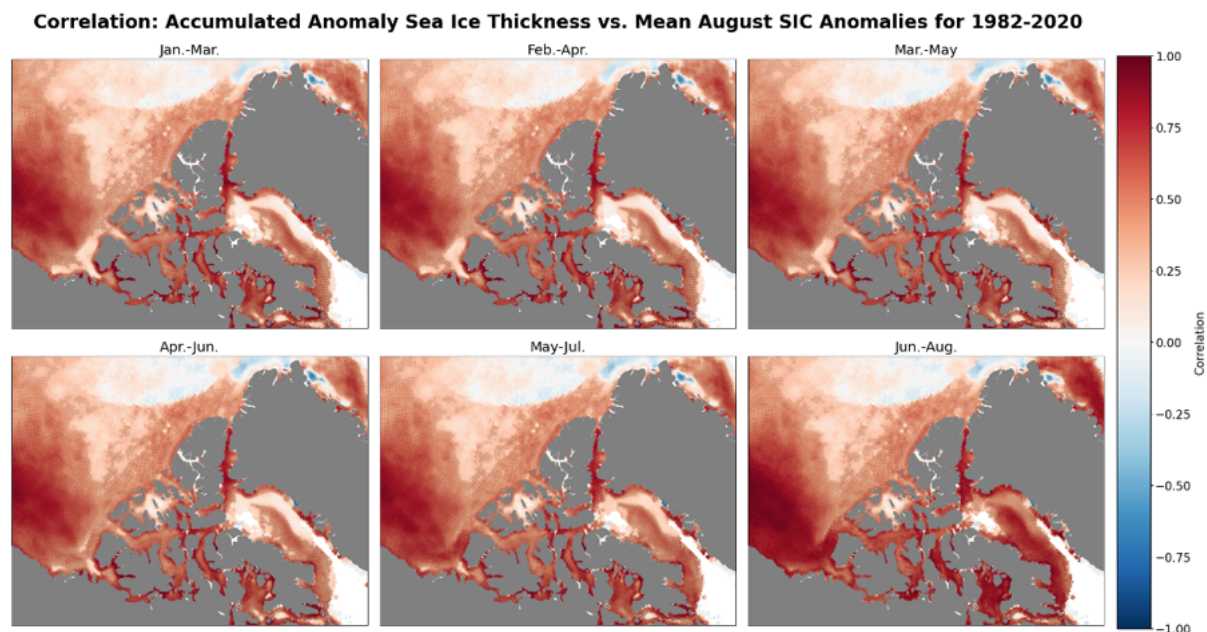


FIGURE 3.14: Sea Ice Thickness correlated with mean August SIC anomalies from 1982 through 2020 for various 3-month periods. Stippling is where p -values ≤ 0.05 .

The composite analysis showed that differences between years with at least one standard deviation higher and lower than the mean August SIC exist in terms of their environmental conditions. The most apparent differences between the low August SIC years and the high August SIC years seems to take form in the spring, with sea ice thickness already showing slight differences in the winter. SIC, thickness, and Two-meter temperature are the strongest and most widespread predictors of August SIC at the earliest points in the year according to the correlation analysis. All three of these predictors seem to have significant correlations in the winter months, with thickness seemingly the strongest predictor of August SIC.

Interestingly, although certain variables may be good predictors of August SIC early in the season, the composite analysis tells us that the strongly +/- August SIC anomaly

years do not begin to differentiate themselves until the Spring in most cases (except for sea ice thickness). Most significant differences in the samples appear in the March through May and the April through June periods, but the correlations seem to show some degree of predictability even earlier in the year for SIC, thickness, Two-meter temperature, and arguably the zonal wind. This is not to say that there is no predictive capability for any variable except for sea ice thickness before the spring, but rather that the spring seems to be a tipping point that can lead to August SICs going towards one extreme or another (at least $\pm 1\sigma$ mean August SIC).

3.5 Part 3: Sea Ice Concentration Prediction

Using the variables analyzed in the previous two parts, the predictability of August SIC can be analyzed using CNNs. Two models were trained on environmental accumulated anomalies from various 3-month periods. The first model is trained on January, February, and March (JFM) accumulated anomalies and the second is trained on May, June, and July (MJJ) accumulated anomalies. The way in which these accumulated anomalies are used to train these models is that the variables' (past SIC, sea ice thickness, zonal and meridional winds, and Two-meter temperature) accumulated anomalies are calculated for each month, but instead of summing the full 3-month period each month is used as a different predictor as input to the model. Simply put, the JFM model is trained/tested on the full dataset from 1982 through 2020, but instead of there being one input for each variable, there are 3, with 15 total predictors (5 for each month). The reason for choosing to separate the 3-month periods into individual months (thereby tripling the

input variables/predictors) is because this will give the model some information as to how the environment may be changing over this 3-month period with respect to each variable. Each model will also have a $1-\sigma$ Gaussian smoothing filter applied to reduce prediction noise and remove pixels that may be abnormal after the model prediction process.

Figure 3.15 shows the correlation between the predictions and the validation of SIC at each point in the NWP region from the years 1982 through 2020. The focus should be on the bottom half of the figure, which is the correlation after a $1-\sigma$ Gaussian smoothing filter was applied to the predictions. Overall, the January, February, and March CNN does not have highly correlated and significant areas of accurate predictions. The area where this model seems to perform the best is within the waterways of the southern routes of the NWP. Flattening the array of predictions and validation, and calculating the root-mean-square error (RMSE) gives a value of 0.198 for the smoothed correlation. This means that on average, there is a deviation of about 20% between the predictions and the validation. Interestingly, when the entire Arctic is included in the prediction, the RMSE goes down to 0.128, or about 13%. This discrepancy is likely due to the fact that the NWP's landmasses and bathymetry differ from most of the other Arctic waters, complicating predictions in the area.

Figure 3.16 shows the correlation between the predictions and the validation of SIC, but this model was trained on May, June, and July anomalies. What becomes apparent right away is this model performs much better than the JFM model. This, of course,

CNN (JFM w/o Fluxes) Model SIC Prediction vs. Validation Correlation

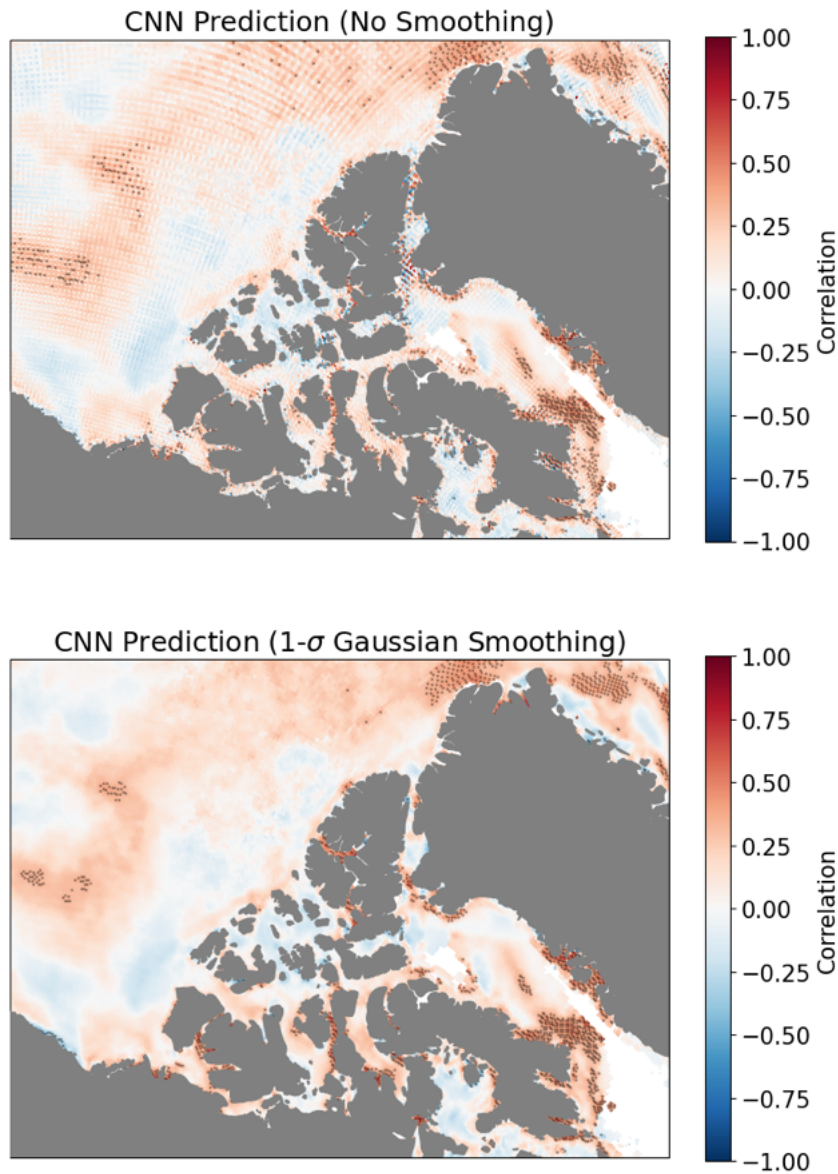


FIGURE 3.15: CNN (trained on JFM accumulated anomalies) predictions and validation are correlated to show where predictions are most accurate. Positive correlations (red) mean the model predictions are positively correlated with validation (this is desired), while negative correlations (blue) mean model predictions are not resolving with validation. The top part of the figure is the correlation in its raw form, but the bottom is the correlation after a $1\text{-}\sigma$ Gaussian smoothing filter was applied to the CNN predictions. Stippling is where $p\text{-values} \leq 0.05$.

CNN (MJJ w/o Fluxes) Model SIC Prediction vs. Validation Correlation

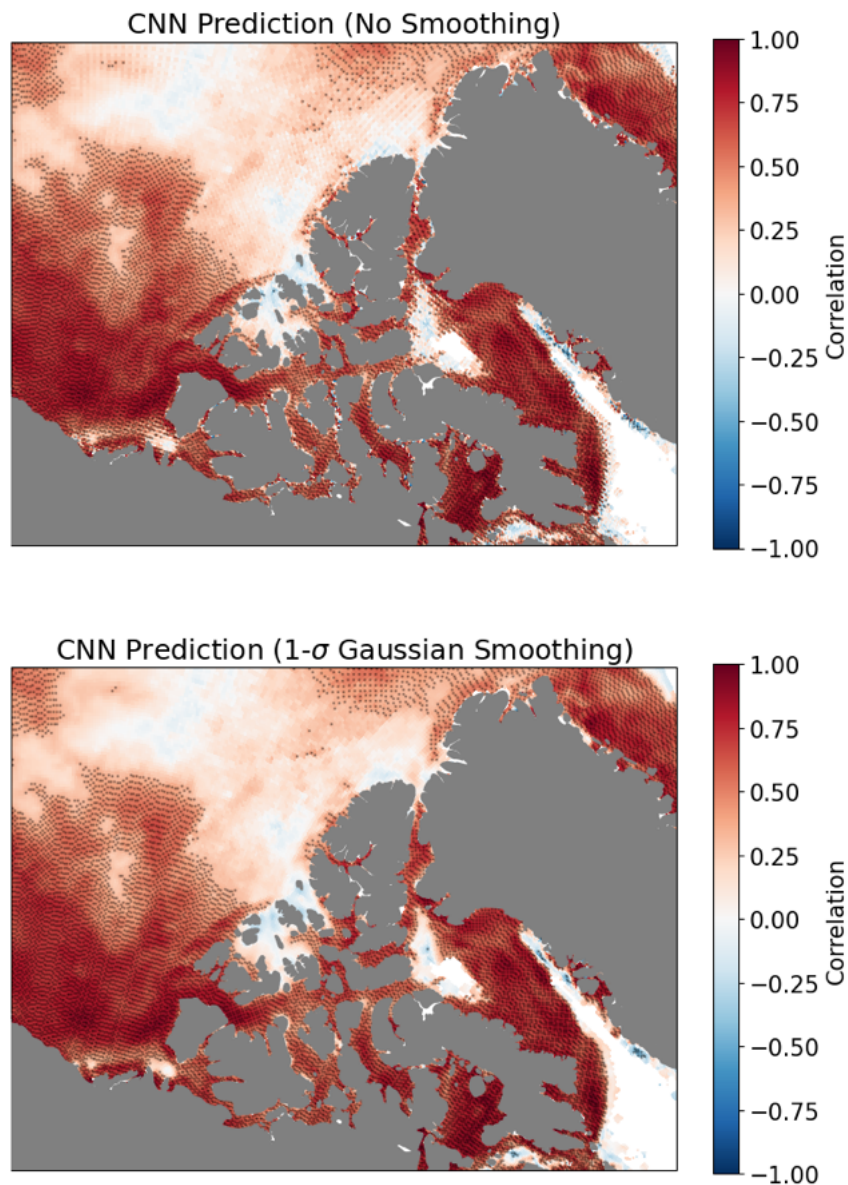


FIGURE 3.16: CNN (trained on MJJ accumulated anomalies) predictions and validation are correlated to show where predictions are most accurate. Positive correlations (red) mean the model predictions are positively correlated with validation (this is desired), while negative correlations (blue) mean model predictions are not resolving with validation. The top part of the figure is the correlation in its raw form, but the bottom is the correlation after a $1\text{-}\sigma$ Gaussian smoothing filter was applied to the CNN predictions. Stippling is where $p\text{-values} \leq 0.05$.

is expected due to the proximity of MJJ to August. It is important to note that the model's best performance is within the NWP and over the Beaufort Sea, which are the regions where maritime vessels would be most likely to traverse. The correlations reach well above 75% in some areas, and almost the entirety of the NWP has significant area. The RMSE of the predictions for the NWP region compared to validation is 0.144, or just under 14.5%. When accounting for the whole Arctic, the RMSE drops to 0.0876, or just under 9%. These errors are still high, but can be improved upon in the future as more predictors and higher resolution data becomes available.

As discussed in [Zeng et al. \(2023\)](#), the Spring Barrier is often associated with lower predictability of SIC before June, but these predictions can be improved by including more variables relating to the surface heat flux. To test whether this is the case, additions will be made to both the JFM and MJJ CNNs. These new models, which include the downwelling shortwave flux at the surface, the upwelling and downwelling longwave flux at the surface, the shortwave cloud radiative forcing at the surface, and the longwave cloud radiative forcing at the surface will be compared to [Figure 3.15](#) and [Figure 3.16](#) to test whether improvements occur in either (or both) of these models.

[Figure 3.17](#) shows some improvement to SIC predictions when compared to [Figure 3.15](#). Though this improvement is not widespread, it is apparent that positive correlations and significant area are far more widespread in the Beaufort Sea region. The RMSE in the NWP region when fluxes are included drops to 0.150 from 0.198 for JFM, an almost 5%

CNN (JFM w/ Fluxes) Model SIC Prediction vs. Validation Correlation

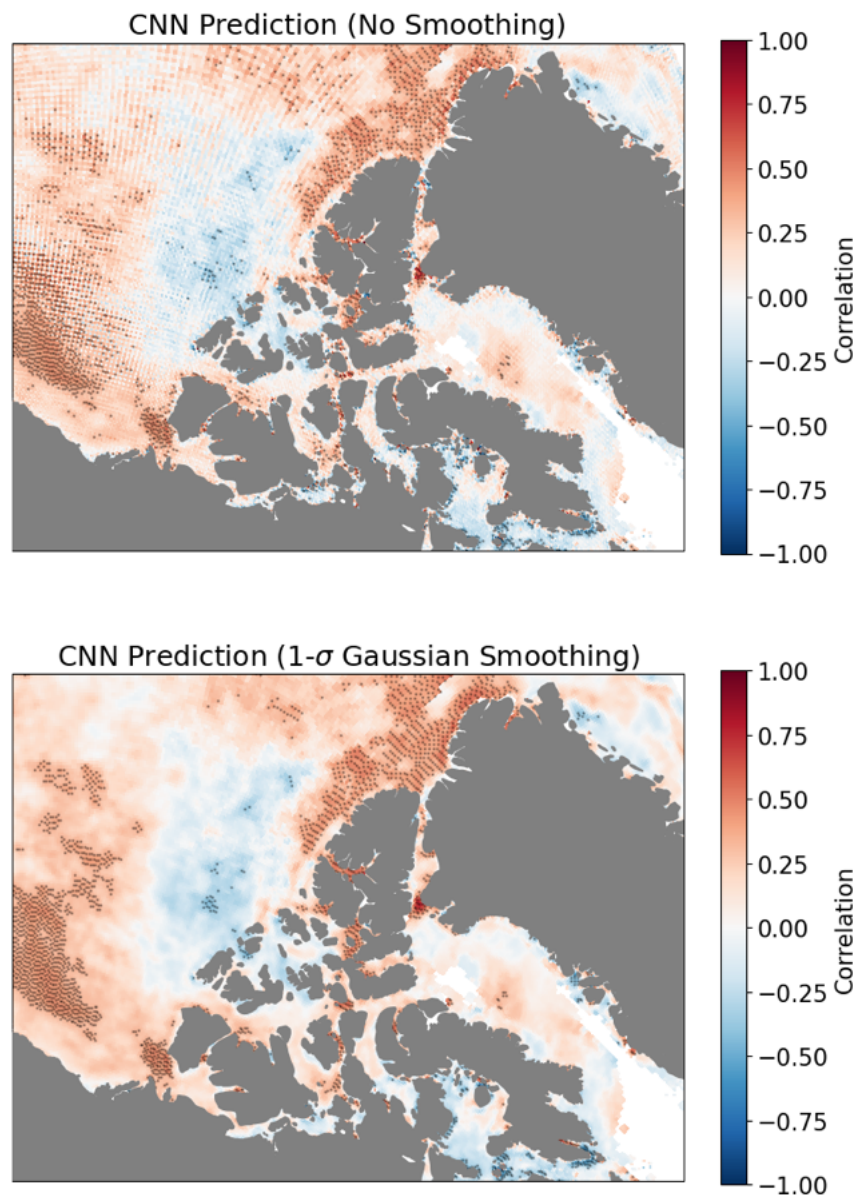


FIGURE 3.17: CNN (trained on JFM accumulated anomalies and including additional flux variables) predictions and validation are correlated to show where predictions are most accurate. Positive correlations (red) mean the model predictions are positively correlated with validation (this is desired), while negative correlations (blue) mean model predictions are not resolving with validation. The top figure is the correlation in its raw form, but the bottom is the correlation after a $1\text{-}\sigma$ Gaussian smoothing filter was applied to the CNN predictions. Stippling is where $p\text{-values} \leq 0.05$.

improvement. For the whole Arctic the RMSE drops to 0.120 from 0.128. It seems that the addition of the heat flux information has contributed to this model improvement.

Figure [3.18](#) shows the MJJ model's correlation, this time with fluxes included. Comparing to Figure [3.16](#), there is not a significant difference between the two figures. In fact, the RMSE in the NWP region went to 0.149 from 0.144 when including fluxes. For the whole Arctic the RMSE is now 0.0986 where it was 0.0876 without the fluxes. It seems that the Spring Barrier can be reduced when using variables related to the heat flux before June, but including them after May does not make much of a difference. In fact, it may add to the error. Of course, all models in this analysis had the same architecture and number of training epochs, so it is likely that the accuracy could be maintained for the MJJ model when using heat flux information by increasing the training time and giving the model more time to learn the connections between the additional variables and SIC. This may be explored in a future analysis.

CNN (MJJ w/ Fluxes) Model SIC Prediction vs. Validation Correlation

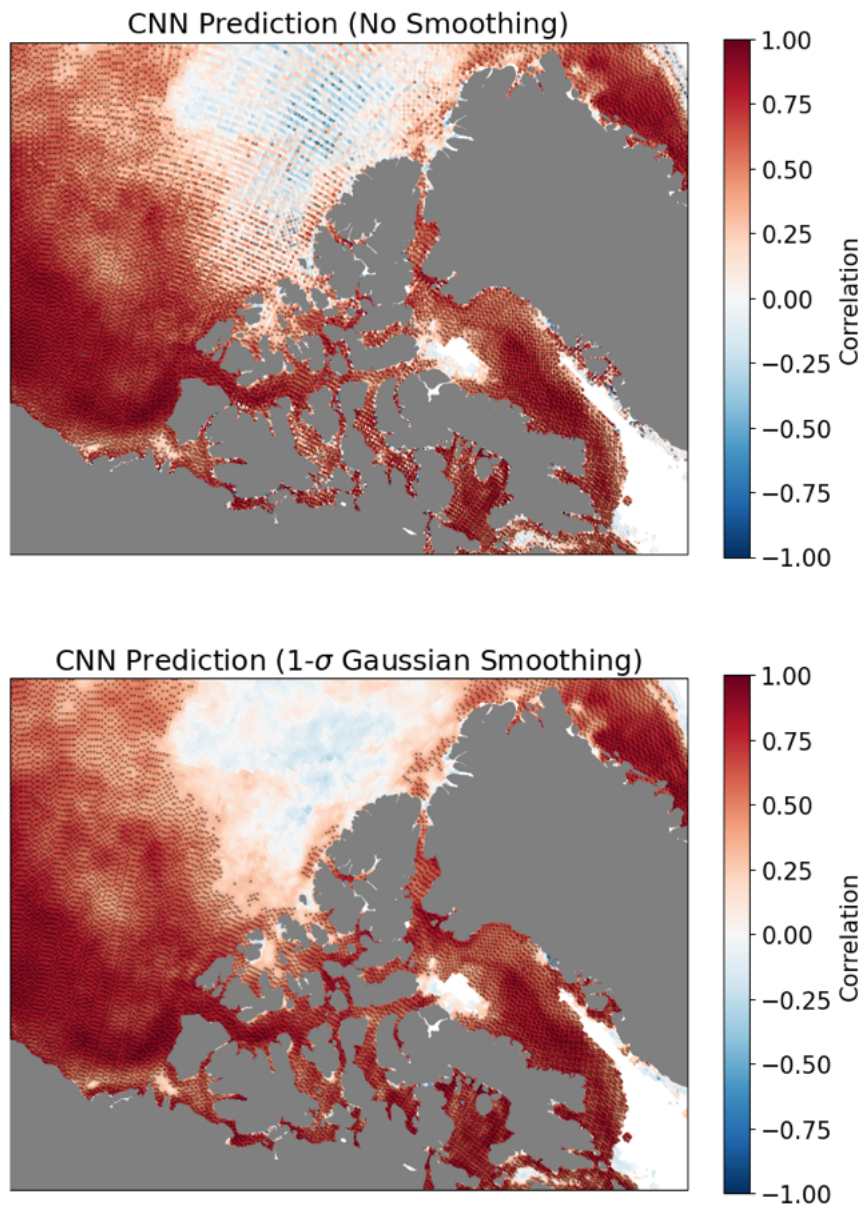


FIGURE 3.18: CNN (trained on MJJ accumulated anomalies and including additional flux variables) predictions and validation are correlated to show where predictions are most accurate. Positive correlations (red) mean the model predictions are positively correlated with validation (this is desired), while negative correlations (blue) mean model predictions are not resolving with validation. The top figure is the correlation in its raw form, but the bottom is the correlation after a $1\text{-}\sigma$ Gaussian smoothing filter was applied to the CNN predictions. Stippling is where $p\text{-values} \leq 0.05$.

Chapter 4

Summary and Conclusions

The Arctic is likely going to experience an increase in maritime activity as the region continues to warm and sea ice amounts decrease, especially in the late-summer. It is for this reason that interest in predicting sea ice concentrations in the Arctic, specifically in the Northwest Passage, has begun to increase. SIC prediction will allow for increased maritime safety in the region, and help reduce the chances of a disastrous situation like an oil spill that would have severe environmental consequences, loss of property, and loss of human life.

Differences between the SIC in the NWP during the summers of 2013 and 2016 were apparent from visible satellite imagery (Figure 1.3), but also when comparing the thermodynamic and dynamic environmental conditions. Temperature differences (shown in the form of freezing degree days, Figure 3.1) showed an increased temperature in 2016 and a

colder temperature in 2013. Not only was the temperature contributing to a difference between these two summers, but the winds in the region showed almost opposite patterns (Figure 3.2). 2013 had a cyclonic wind pattern that push sea ice into the NWP region, raising SICs. 2016 saw an anticyclonic pattern that would lower the SIC by transporting sea ice out of the NWP. It was the differences between 2013 and 2016 that encouraged a search for other years that had at least one standard deviation higher or lower of average August SIC anomalies. The result was two samples of six years each that served as the two samples for the composite analysis.

Compositing the accumulated anomalies of the variables of interest (Two-meter temperature, 10-meter zonal and meridional winds, sea ice thickness, and past sea ice concentrations from earlier in the year) showed clear differences between the two samples. These differences became apparent the earliest when looking at the sea ice thickness, but the Two-meter temperature and SIC anomalies all showed significant differences becoming largely apparent in the spring. The zonal wind was shown to be opposite between the two samples as well, with a net eastward effect of the wind during the high sea ice years, and a westward effect during the low sea ice years. The meridional wind's pattern was less clear.

The correlation analysis is where the direct relationships between the environmental variables and the average August SIC anomalies were analyzed by calculating the Pearson correlation coefficient at each grid point between the August SIC anomalies and each variable of interest separately. The results showed that the sea ice thickness, SIC, and the

Two-meter temperature were the strongest predictors of August SIC anomalies because they began to show correlations in the early spring and even in the winter for sea ice thickness and Two-meter temperature. The closer to August the thinner the ice is, and in the late spring this is when the zonal wind became most correlated with August SIC anomalies, particularly along the western axis of the Canadian Archipelago.

Based on the composite and correlation analyses, it becomes apparent that certain variables may be good predictors of average August SIC anomalies earlier in the year, but the strongly +/- August SIC anomaly years do not begin to differentiate themselves until the spring in most cases (except for sea ice thickness). Most significant differences between the low and high SIC years begin to appear in March through May in the composite analysis, but the correlations show significant correlations even earlier than this period. Predictability of August SIC likely exists in more of these variables than just the sea ice thickness earlier in the year, but the extreme years with at least one standard deviation greater/lower average August SIC do not present themselves until the spring, which is the time of the year that acts as a tipping point for extreme anomalies with respect to SIC in the NWP region.

From here, CNNs were constructed to predict August SICs from the variables of interest. Obviously, the closer to August the environmental conditions are that are used to predict August SIC, the more accurate the model will be. This becomes increasingly apparent when comparing Figure [3.15](#) and Figure [3.16](#). However, predictions from earlier in the year need to overcome the “Spring Barrier” as it is referred to in [Bonan](#)

et al. (2019). This barrier often decreases SIC predictability before June, but it is said including environmental information about the heat flux in the training process can increase the accuracy of early season predictions (Zeng et al., 2023). To test this, five additional variables were included to try and improve predictions early in the year from the JFM model. These additional variables are the downwelling shortwave flux at the surface, the upwelling and downwelling longwave flux at the surface, the shortwave cloud radiative forcing at the surface, and the longwave cloud radiative forcing at the surface. It was found that the accuracy of predictions increased for the early-year JFM model when these additional variables are included, but interestingly, the accuracy was reduced slightly when including these variables in the MJJ model.

The main conclusions are:

1. Characteristic thermodynamic and dynamic environments exist when comparing low and high August SIC years. Particularly, the sea ice thickness, the Two-meter temperature, and the prior SIC anomalies all show differences in the early spring, or even in the winter in the case of the sea ice thickness (to the southwest of Banks Island).
2. The best, and earliest, predictor of August SIC is the sea ice thickness. The Two-meter temperature also shows strong predictive capability early in the year. The prior SIC anomalies and zonal wind become better predictors once the late-spring is included.

3. Although there is predictability of August SIC before the spring for certain variables, the strongly +/- August SIC anomaly years do not present themselves until the spring.
4. Simple convolutional neural networks are able to predict average August SICs at varying degrees of accuracy depending on the time of the year of the predictors. The closer to August the predictors are, the more accurate the August SIC predictions will be. However, early season models will increase in accuracy when including variables related to the radiative/heat flux at the surface. This was apparent when comparing the JFM model without these fluxes (Figure 3.15) to the model that included them (Figure 3.17).

Bibliography

- Abadi, M., P. Barham, J. Chen, Z. Chen, A. Davis, J. Dean, M. Devin, S. Ghemawat, G. Irving, M. Isard, M. Kudlur, J. Levenberg, R. Monga, S. Moore, D. G. Murray, B. Steiner, P. Tucker, V. Vasudevan, P. Warden, M. Wicke, Y. Yu, and X. Zheng, 2016: Tensorflow: A system for large-scale machine learning. *12th USENIX Symposium on Operating Systems Design and Implementation (OSDI 16)*, 265–283.
- Andersen, S., R. Tonboe, L. Kaleschke, G. Heygster, and L. T. Pederson, 2007: Intercomparison of passive microwave sea ice concentration retrievals over the high-concentration Arctic sea ice. *Journal of Geophysical Research: Oceans*, **112**, 2156–2202, doi:10.1029/2006JC003543.
- Andersson, T. R., J. S. Hosking, M. Perez-Ortiz, B. Paige, and A. Elliott, 2021: Seasonal Arctic sea ice forecasting with probabilistic deep learning. *Nature Communications*, **12**, 5124, doi:10.1038/s41467-021-25257-4.
- Assel, R. A., 1980: Maximum Freezing Degree-Days as a Winter Severity Index for the Great Lakes, 1897–1977. *Monthly Weather Review*, **108**, 1440–1445, doi:https://doi.org/10.1175/1520-0493(1980)108<1440:MFDDAA>2.0.CO;2.

- Bonan, D. B., M. Bushuk, and M. Winton, 2019: A Spring Barrier for Regional Predictions of Summer Arctic Sea Ice. *Geophysical Research Letters*, **46**, 5935–5947, doi:10.1029/2019GL082947.
- Chollet, F., 2021: *Deep learning with Python (Second Edition)*. Manning, Shelter Island, NY.
- Headland, R. K., 2022: The Scott Polar Research Institute - Transits 2022. *The North West Passage*, <https://thenorthwestpassage.info/spri-transits-2020>.
- Hersbach, H. and Coauthors, 2020: The ERA5 global reanalysis. *Quarterly Journal of the Royal Meteorological Society*, **146**, 1999–2049, doi:10.1002/qj.3803.
- Hoffman, L., M. R. Mazloff, S. T. Gille, D. Giglio, C. M. Bitz, P. Heimbach, and K. Matsuyoshi, 2023: Machine Learning for Daily Forecasts of Arctic Sea Ice Motion: An Attribution Assessment of Model Predictive Skill. *Artificial Intelligence for the Earth Systems*, **2**, 2769–7525, doi:10.1175/AIES-D-23-0004.1.
- Howell, S. E. L., D. G. Babb, J. C. Landy, and M. Brady, 2022: Multi-Year Sea Ice Conditions in the Northwest Passage: 1968–2020. *Atmosphere-Ocean*, **0**, 1–15, doi:10.1080/07055900.2022.2136061.
- Kapsch, M.-L., R. G. Graversen, T. Economou, and M. Tjernstrom, 2014: The importance of spring atmospheric conditions for predictions of the Arctic summer sea ice extent. *Geophysical Research Letters*, **41**, 5288–5296, doi:10.1002/2014GL060826.

- Kern, S., T. Lavergne, L. T. Pederson, R. T. Tonboe, L. Bell, M. Meyer, and L. Zeigermann, 2022: Satellite passive microwave sea-ice concentration data set intercomparison using Landsat data. *The Cryosphere*, **16**, 349–378, doi:10.5194/tc-16-349-2022.
- Key, J., X. Wang, Y. Liu, R. Dworak, and A. Letterly, 2016: The ERA5 global reanalysis. *Remote Sensing*, **167**, doi:10.3390/rs8030167.
- Kimura, N., A. Nishimura, Y. Tanka, and H. Yamaguchi, 2013: Influence of winter sea-ice motion on summer ice cover in the Arctic. *Polar Research*, **32**, 20193, doi:10.3402/polar.v32i0.20193.
- Klauz, A. V., I. E. Frolov, V. V. Kharitonov, and A. A. Shaeva, 2021: Methodology for calculating the criteria of economic efficiency of investments in nuclear icebreakers. *Nuclear Energy and Technology*, **7**, 333–339, doi:10.3897/nucet.7.78501.
- Levy, R., 2007: Northwest Passage Open. *NASA Earth Observatory*, <https://earthobservatory.nasa.gov/images/18962/northwest-passage-open>.
- Meier, W. N., F. Fetterer, A. K. Windnagel, J. S. Stewart, and T. Stafford, 2024: NOAA/NSIDC Climate Data Record of Passive Microwave 12.5 km Sea Ice Concentration, Version 5. *NSIDC: National Snow and Ice Data Center*, CDR Sea Ice Concentration, doi:<https://doi.org/10.7265/10.7265/rjzb-pf78>.
- Skripnuk, D. F., I. O. Iliyushchenko, S. V. Kulik, and M. M. Stepanova, 2020: Analysis of the current state of the Northern Sea Route and the potential development of the

icebreaker fleet. *IOP Conference Series: Earth and Environmental Science*, **539**, 1–7, doi:10.1088/1755-1315/539/1/012129.

Snider, D., 2016: Crystal Serenity – A New Chapter in Arctic Shipping or Just “Doing it Right”? *Arctic Yearbook*, <https://arcticyearbook.com/arctic-yearbook/2016/2016-commentaries/194-crystal-serenity-a-new-chapter-in-arctic-shipping-or-just-doing-it-right>.

Somanathan, S., P. C. Flynn, and J. Szymanski, 2006: The Northwest Passage: A Simulation. *Proceedings of the 2006 Winter Simulation Conference*, 1578–1585, doi:10.1109/WSC.2006.322929.

Stroeve, J. C., T. Markus, L. Boisvert, J. Miller, and A. Barrett, 2014: Changes in Arctic melt season and implications for sea ice loss. *Geophysical Research Letters*, **41**, 1216–1225, doi:10.1002/2013GL058951.

Wang, C., M. Ding, Y. Yang, T. Wei, and T. Dou, 2022: Risk Assessment of Ship Navigation in the Northwest Passage: Historical and Projection. *Sustainability*, **14**, 5591, doi:10.3390/su14095591.

Wang, Q., S. Danilov, L. Mu, D. Sidorenko, and C. Wekerle, 2021: Lasting impact of winds on Arctic sea ice through the ocean’s memory. *The Cryosphere*, **15**, 4703–4725, doi:10.5194/tc-15-4703-2021.

- Wei, T., Q. Yan, W. Qi, M. Ding, and C. Wang, 2020: Projections of Arctic sea ice conditions and shipping routes in the twenty-first century using CMIP6 forcing scenarios. *Environmental Research Letters*, **15**, 104079, doi:10.1088/1748-9326/abb2c8.
- Yu, M., P. Lu, Z. Li, Z. Li, Q. Wang, X. Cao, and X. Chen, 2021: Sea ice conditions and navigability through the Northeast Passage in the past 40 years based on remote-sensing data. *International Journal of Digital Earth*, **14**, 555–574, doi:10.1080/17538947.2020.1860144.
- Zeng, J., Q. Yang, X. Li, X. Yuan, M. Bushuk, and D. Chen, 2023: Reducing the Spring Barrier in Predicting Summer Arctic Sea Ice Concentration. *Geophysical Research Letters*, **50**, e2022GL102115, doi:10.1029/2022GL102115.